

ZIRCONIUM, BARIUM, LANTHANUM AND EUROPIUM ABUNDANCES IN OPEN CLUSTERS

HEATHER R. JACOBSON^{1,2,3}

Department of Physics & Astronomy, Michigan State University, East Lansing, MI 48823; jacob189@msu.edu

EILEEN D. FRIEL

Department of Astronomy, Indiana University, Bloomington, IN 47405; efriel@indiana.edu

Published in The Astronomical Journal, 2013, 145, 107

ABSTRACT

We present an analysis of the s-process elements Zr, Ba, and La and the r-process element Eu in a sample of 50 stars in 19 open clusters. Stellar abundances of each element are based on measures of a minimum of two lines per species via both equivalent width and spectrum synthesis techniques. We investigate cluster mean neutron capture abundance trends as a function of cluster age and location in the Milky Way disk and compare them to results found in other studies in the literature. We find a statistically significant trend of increasing cluster [Ba/Fe] as a function of decreasing cluster age, in agreement with recent findings for other open cluster samples, supporting the increased importance of low mass AGB stars to the generation of s-process elements. However, the other s-process elements, [La/Fe] and [Zr/Fe] do not show similar dependences, in contrast to theoretical expectations and the limited observational data from other studies. Conversely, cluster [Eu/Fe] ratios show a slight increase with increasing cluster age, although with marginal statistical significance. Ratios of [s/r]-process abundances, [Ba/Eu] and [La/Eu], however, show more clearly the increasing efficiency of s-process relative to r-process enrichment in open cluster chemical evolution, with significant increases among younger clusters. Lastly, cluster neutron capture element abundances appear to be independent of Galactocentric distance. We conclude that a homogeneous analysis of a larger sample of open clusters is needed to resolve the apparent discrepant conclusions between different studies regarding s-process element abundance trends with age to better inform models of galactic chemical evolution.

Subject headings: Galaxy: abundances — stars: abundances

1. INTRODUCTION

It is well established that open clusters do not exhibit an age-metallicity relation (e.g., Friel 1995, Carrera & Pancino 2011). The fact that old, super-solar metallicity clusters (e.g., NGC 188, NGC 6791) and young, sub-solar metallicity clusters (e.g., NGC 2324) can be found in the disk seems to indicate that the location of a cluster's birth is more important than when it formed in terms of the signatures of disk chemical evolution imprinted on its stars (Salaris et al. 2004). This is seen in the radial metallicity gradient in the disk, as traced by open clusters, cepheids, and other populations (e.g., Yong et al. 2012). The distribution of abundances of other chemical elements (such as the alpha-, light and Fe-peak elements) also appear to trace that of iron very well, with open clusters having [X/Fe] ratios that are essentially independent of cluster age and galactocentric radius (R_{gc} ; e.g., Magrini et al. 2009, Friel et al. 2010)⁴.

The findings of studies of open cluster neutron-capture element abundances, however, stand in exciting contrast to the behavior seen for the other elements. Neutron capture species, generated in low mass AGB stars and massive stars via the strong and weak s-processes and (likely) in type II supernovae via the r-process (e.g., Busso et al. 1999, Busso et al. 2001, Sneden et al. 2008, Pignatari et al. 2010), have only recently been studied in decently large, homogeneous samples of open clusters, and are further useful probes of the mass range of stars that contributed to the chemical evolution of the disk. D'Orazi et al. (2009) reported an unexpected trend of increasing cluster [Ba/Fe] with decreasing cluster age that cannot be explained by chemical evolution models using standard AGB star s-process yields. An analysis of the s-process elements Y, Ce, Zr and La in open clusters by Maiorca et al. (2011) found an analogous trend for these elements, though it should be noted that the result is most robust for Y and Ce. Given that this trend is seen for both light s-elements (Y, Zr) and heavy s-process elements (Ba, La, Ce) in these studies, one can conclude that the cause of this increased enrichment in younger stars affects all elements produced by the main s-process in the same way.

in galaxy disks via various mechanisms can greatly influence radial metallicity gradients (e.g., Roškar et al. (2008) and Loebman et al. (2011)), to our knowledge it has not been demonstrated that open clusters are subject to radial migration. It goes without saying the usefulness of cluster element abundance trends with R_{gc} as probes of disk chemical evolution hinges on the answer to this question.

¹ National Science Foundation Astronomy and Astrophysics Postdoctoral Fellow.

² Visiting Astronomer, Kitt Peak National Observatory, National Optical Astronomy Observatory, which is operated by the Association of Universities for Research in Astronomy (AURA) under cooperative agreement with the National Science Foundation.

³ Current address: Massachusetts Institute of Technology, Kavli Institute for Astrophysics and Space Research, 77 Massachusetts Ave., Cambridge, MA, 02139; hrj@mit.edu

⁴ This discussion ignores the possible role of radial migration in shaping trends of cluster abundances (and age) with R_{gc} . While recent simulations have indicated that radial migration of stars

Table 1
Cluster Sample

Cluster	Age ^a (Gyr)	d (kpc)	R_{gc} ^b (kpc)	Ref. ^c	No. of Stars	Telescope
Be 17	10.1	2.7	11.7	F05	3	KPNO 4m
Be 18	5.7	5.4	13.7	Y12	2	Keck
Be 21	2.2	6.2	14.7	Y12	2	Keck
Be 22	4.3	6.2	14.4	Y12	2	Keck
Be 32	5.9	3.2	11.6	FJP10	2, 2	KPNO 4m, Keck
Be 39	7.0	4.3	11.9	FJP10	4	KPNO 4m
M 67	4.30	0.8	9.1	FJP10	3	KPNO 4m
NGC 188	6.3	1.7	9.4	FJP10	4	KPNO 4m
NGC 1193	4.2	5.8	13.6	FJP10	1	HET
NGC 1245	1.1	3.0	11.1	J11	4	KPNO 4m
NGC 1817	1.1	1.5	10.0	J09	2	KPNO 4m
NGC 1883 ^d	0.7	3.9	12.3	J09	2	KPNO 4m
NGC 2141	2.4	3.9	12.2	J09	2	KPNO 4m
NGC 2158	1.9	4.0	12.8	J09	1	KPNO 4m
NGC 2194	0.9	1.9	10.3	J11	2	KPNO 4m
NGC 2355	0.8	1.9	10.3	J11	3	KPNO 4m
NGC 6939	1.2	1.8	8.4	A04	4	KPNO 4m
NGC 7142	4.0	1.9	9.2	J08	4	KPNO 4m
PWM 4	7.0	7.2	13.3	Y12	1	Keck

^a Adopted from Salaris et al. (2004)

^b $R_{\odot} = 8.5$ kpc

^c References for distances: A04: Andreuzzi et al. (2004); F05 = Friel et al. (2005); FJP = Friel et al. (2010); J08 = Jacobson et al. (2008); J09 = Jacobson et al. (2009); J11 = Jacobson et al. (2011); Y12 = Yong et al. (2012)

^d NGC 1883 is not included in the sample of Salaris et al.. This value is taken from Villanova et al. (2007) (uncertainty 0.07 Gyr).

D’Orazi et al. interpreted this anticorrelation with age as an indication that low-mass ($<1.5 M_{\odot}$) AGB stars contributed more to the chemical evolution of the disk than theoretical models previously indicated. This scenario has been further explored by Maiorca et al. (2012), who presented revised s-process production models for low-mass stars in which the neutron source was larger by a factor of four than in previous models. Applying the s-process yields produced by this model in a chemical evolution study, they could reasonably reproduce the observed trend of $[s/Fe]$ with age seen by open clusters.

It is very intriguing that a recent study of solar-type stars in the solar neighborhood (for which there are Hipparcos distances and therefore, isochrone ages) has also found trends of increasing $[s/Fe]$ with decreasing age. Indeed, the dwarf stars in the study by da Silva et al. (2012) show a very similar pattern of $[s/Fe]$ with age to the open clusters in the D’Orazi et al. and Maiorca et al. studies, most notably for the elements Ba and Zr, and especially for stars younger than the age of the Sun (see their Figure 11). That said, the results of another open cluster study show conflicting results. Yong et al. (2012) presented a homogeneous chemical abundance study of 11 open clusters, and in combination of results from the literature, investigated trends of cluster element abundances as a function of R_{gc} and cluster age⁵. While they found trends of increasing $[Ba/Fe]$ and $[Zr/Fe]$ with decreasing cluster age, they were not as strong as those found by D’Orazi et al. and Maiorca et al. (hereafter

D09 and M11). What is more, they found a trend of increasing $[La/Fe]$ with *increasing* cluster age, in the direct opposite sense of the M11 result.

Given the important role open clusters perform in tracing the chemical evolution of the disk, it is imperative to firmly establish the existence and behavior of their element abundance trends with age. To that end, we present here an analysis of neutron capture element abundances in a sample of 19 open clusters spanning in age from ~ 700 Myr to 10 Gyr. Our study has many stars in common with those of Yong et al. (2012; hereafter Y12), but we have undertaken a completely independent analysis of them. Furthermore, only two clusters in our sample are common to the studies of D09 and M11, and therefore this study is an independent investigation of cluster abundance trends with age. The elements investigated in this study are primarily s-process elements: Zr, Ba and La. We also report abundances for the r-process element europium (Eu).

2. SAMPLE

The cluster sample used in this work is shown in Table 1. Much of our stellar sample has been presented in previous work, and is comprised of echelle spectra from KPNO 4m and Hobby-Eberly telescopes (see Friel et al. 2005, 2010, Jacobson et al. 2008, 2009). This sample includes confirmed radial velocity cluster member red clump and giant stars in the clusters Be 17 (3 stars), Be 32 (2 stars), Be 39 (4 stars), M 67 (3 stars), NGC 188 (4 stars), NGC 1193 (1 star), NGC 1817 (2 stars), NGC 1883 (2 stars), NGC 2141 (2 stars⁶), NGC 2158 (1

⁵ It should be noted for the present discussion that only a subset of the literature sample they examined had neutron capture element abundances reported, a large fraction of which were from their own work (see their Table 13), and so the usual risks inherent in interpreting trends in inhomogeneous datasets are not so important here.

⁶ The spectrum of star 1348 was obtained by Yong et al. 2005 using a similar spectrograph setup to the data described here. This spectrum was kindly given to us by D. Yong (2008, private communication) and was analyzed in Jacobson et al. (2009).

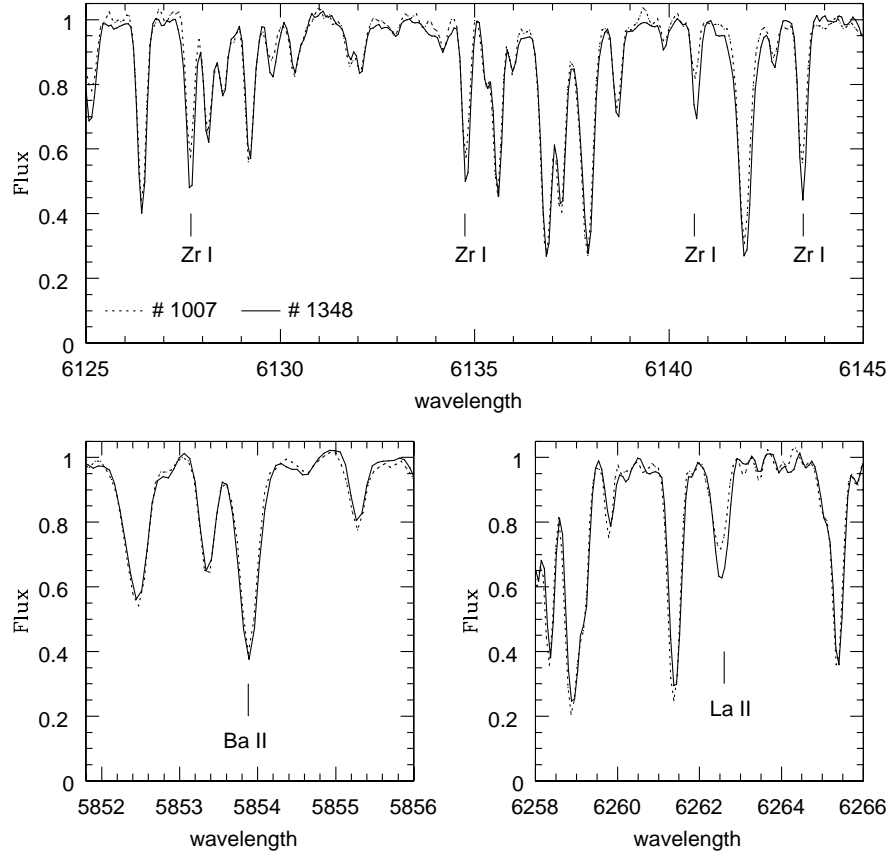


Figure 1. Sample portions of the spectra for stars 1007 (dashed line) and 1348 (solid line) of NGC 2141. The two stars have identical atmospheric parameters and metallicities, but 1348 shows enhanced Zr and La abundances relative to 1007, although their Ba and Eu line strengths are very similar.

star) and NGC 7142 (4 stars). The reader is referred to references above for details regarding the observations, reductions, and analysis of these data and information about the stellar targets.

Additional high resolution spectra of stars in clusters Be 18, Be 21, Be 22, Be 32, and PWM 4 obtained with the HIRES spectrograph on Keck were kindly given to us by D. Yong (two stars in each cluster save one in PWM 4). These outer disk clusters serve as an important supplement to our sample, and a comparison of the analysis here to that presented by Y12 provides important information about systematic differences between different cluster samples in the literature along the lines investigated by us previously (see Appendix in Friel et al. 2010, hereafter FJP10). We refer the reader to Y12 for details regarding the observations and reductions of these spectra.

We obtained new observations of stars in open clusters NGC 1245, NGC 2194, NGC 2355 and NGC 6939 using the echelle spectrograph on the KPNO 4m Mayall telescope in 2010 November. Cluster radial velocity members were selected for high resolution multi-order spectroscopic follow-up from the sample of Jacobson et al. (2011). These data are similar to those obtained by us in previous runs (e.g., FJP10): the long red camera along with the 316 line mm^{-1} grating and a 1" slit resulted in spectra with resolving power $R(\lambda/\Delta\lambda) \sim 28,000$. The

full wavelength range is 5000-8100 Å across 24 orders. Typically 3-6 exposures of no more than 2700 s were obtained for each target to minimize the impact of cosmic rays. In addition, high signal-to-noise (S/N) spectra of radial velocity standard stars and early type stars (used for subtraction of telluric lines) were obtained each night, along with the standard bias, dome flat, and arc lamp calibration frames.

These data were reduced using standard IRAF⁷ procedures, as described in FJP10. After bias subtraction, scattered light removal and flat field division, individual data frames were processed through “L. A. Cosmic”⁸ to remove cosmic rays (van Dokkum 2001; spectroscopic version). Individual orders were then extracted and converted to one-dimensional spectra and dispersion corrected. Individual object spectra were combined to form a single, high S/N spectrum for each star and then continuum-normalized. Signal-to-noise (S/N) ratios of the summed spectra range from 60 to 120 per pixel, with an average value of 80 per pixel. For more information about the stellar targets, such as photometry and radial velocity, please see Jacobson et al. (2011) and

⁷ IRAF is distributed by the National Optical Astronomy Observatory, which is operated by the Association of Universities for Research in Astronomy, Inc., under cooperative agreement with the National Science Foundation.

⁸ See <http://www.astro.yale.edu/dokkum/lacosmic/>

Table 2
Stellar Atmospheric Parameters & Fe abundances

Cluster	Star	T_{eff} (K)	$\log g$ (dex)	v_t (km s $^{-1}$)	[Fe I/H] dex	σ dex	# lines	[Fe II/H] dex	σ (dex)	# lines
Be 18	1163	4650	2.3	1.15	-0.30	0.08	67	-0.31	0.12	8
Be 18	1383	4400	1.9	1.30	-0.34	0.09	71	-0.33	0.18	8
Be 21	50	4650	2.1	1.20	-0.14	0.09	67	-0.22	0.08	9
Be 21	51	4520	1.9	1.40	-0.28	0.13	70	-0.26	0.11	9
Be 22	414	4400	2.1	1.25	-0.24	0.12	68	-0.24	0.12	9
Be 22	643	4000	1.1	1.50	-0.30	0.33	64	-0.26	0.26	6
Be 17	265	4500	2.1	1.40	-0.13	0.14	72	-0.10	0.16	10
Be 17	569	4300	1.5	1.50	-0.11	0.16	73	-0.11	0.16	11
Be 17	1035	4300	1.7	1.50	-0.13	0.15	73	-0.19	0.15	11
Be 32	2	4100	1.0	1.50	-0.29	0.14	72	-0.35	0.27	11
Be 32	4	4100	1.0	1.50	-0.33	0.14	72	-0.41	0.26	11
Be 32	16	4900	2.7	1.00	-0.26	0.10	63	-0.21	0.15	9
Be 32	18	5000	2.7	1.30	-0.19	0.13	66	-0.21	0.12	9
Be 39	3	4200	1.6	1.50	-0.15	0.12	64	-0.14	0.14	11
Be 39	5	4450	1.9	1.40	-0.11	0.14	69	-0.16	0.18	11
Be 39	12	4750	2.3	1.40	-0.12	0.17	68	-0.17	0.07	11
Be 39	14	4750	2.3	1.40	-0.15	0.15	70	-0.13	0.21	11
M 67	105	4450	2.1	1.50	+0.03	0.12	64	-0.01	0.21	11
M 67	141	4700	2.4	1.50	+0.09	0.12	65	+0.07	0.22	11
M 67	170	4300	1.7	1.50	+0.02	0.14	60	+0.00	0.28	11
N 1193	282	4700	2.2	1.50	-0.17	0.14	65	-0.24	0.16	10
N 1245	10	5000	2.2	1.20	-0.01	0.16	69	-0.02	0.21	11
N 1245	125	4800	2.5	1.50	+0.06	0.18	66	+0.04	0.12	11
N 1245	160	4800	2.5	1.30	+0.03	0.17	63	+0.03	0.21	11
N 1245	382	4800	2.3	1.50	+0.00	0.13	71	-0.02	0.15	11
N 1817	73	4850	2.5	1.40	-0.04	0.12	73	-0.07	0.13	11
N 1817	79	5100	2.6	1.50	-0.06	0.14	73	-0.13	0.11	11
N 188	532	4800	2.9	1.50	+0.06	0.19	70	-0.01	0.11	11
N 188	747	4600	2.6	1.50	+0.13	0.19	70	+0.13	0.21	11
N 188	919	4400	2.2	1.50	+0.14	0.19	61	+0.15	0.16	10
N 188	1224	4700	2.9	1.50	+0.13	0.18	71	+0.12	0.20	11
N 1883	8	4500	1.5	1.60	-0.03	0.13	59	-0.04	0.20	11
N 1883	9	4600	1.7	1.60	-0.04	0.13	61	-0.06	0.19	11
N 2141	1007	4100	1.2	1.60	-0.09	0.16	59	-0.07	0.16	11
N 2141	1348	4100	1.2	1.50	-0.09	0.18	47	-0.08	0.18	8
N 2158	4230	4400	1.5	1.50	-0.05	0.15	58	-0.11	0.18	11
N 2194	55	5100	2.5	1.40	-0.06	0.14	70	-0.12	0.17	11
N 2194	57	5100	2.2	1.40	-0.06	0.16	70	-0.11	0.18	11
N 2355	144	5300	3.3	1.30	-0.14	0.21	69	-0.18	0.22	11
N 2355	398	5200	2.1	1.90	+0.05	0.13	71	+0.01	0.20	11
N 2355	668	5100	2.6	1.30	-0.04	0.13	71	-0.05	0.15	11
N 6939	121	4200	1.5	1.60	+0.00	0.22	61	+0.02	0.18	11
N 6939	190	5000	2.6	1.40	+0.15	0.17	71	+0.11	0.21	11
N 6939	212	4300	1.7	1.50	+0.03	0.15	65	+0.07	0.15	11
N 6939	31	4000	0.9	1.50	-0.02	0.18	61	+0.04	0.26	11
N 7142	196	4500	2.2	1.40	+0.08	0.15	55	+0.10	0.14	11
N 7142	229	4300	1.7	1.50	+0.05	0.15	50	+0.01	0.12	11
N 7142	377	4450	2.0	1.50	+0.08	0.13	56	+0.03	0.13	11
N 7142	421	4800	2.5	1.50	+0.10	0.14	60	+0.08	0.14	11
PWM 4	RGB 1	4000	1.2	1.50	-0.18	0.16	61	-0.12	0.30	8

Jacobson et al. (2007) (for NGC 6939).

We carried out a detailed chemical abundance analysis of these stars using the same methods and line list as described here and in our previous work (see FJP10; updated $\log gf$'s for use with MOOG2010, as described below) for elements Fe, Na, Mg, Al, Si, Ca, Ti, Cr, Co, Ni, Zr, Ba, La and Eu. Here, we present the results for Fe and the neutron capture elements, and stellar atmospheric parameters; the other element abundances will be presented in a future paper (Jacobson et al., in prep.).

All told, the total sample contains 50 stars in 19 clusters, with a maximum of four stars per cluster. Figure 1 shows portions of stellar spectra with absorption features of interest identified. Unfortunately, such small numbers of stars per cluster are insufficient to assess the true dispersions of element abundances in open clusters,

and any conclusions we draw from their analysis are vulnerable to the presence of “pathological” stars that are either non cluster members or just outliers. We have WIYN-Hydra single-order multi-object spectroscopy of stars in nine clusters in this study, as well as five others (Jacobson et al. 2007, 2011, Friel et al. in prep.), that include La and Zr absorption features for as many as 30 confirmed members per cluster. We will explore internal cluster abundance dispersions for La and Zr in a future paper.

3. ANALYSIS

3.1. Atmospheric parameters and [Fe/H]

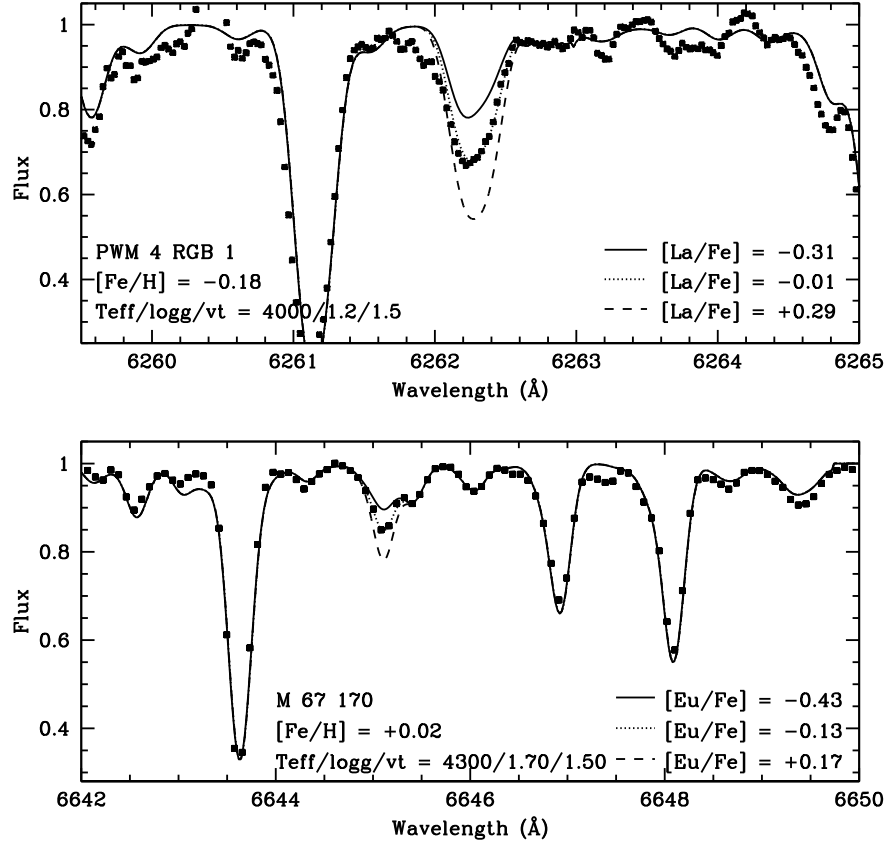


Figure 2. Example syntheses of the La II 6262 feature in star PWM 4 RGB 1 (top panel) and the Eu II 6645 feature in star M 67 170 (bottom panel).

In this work, we used the 2010 version of MOOG (Snedden 1973) and spherical MARCS⁹ model atmospheres (Gustafsson et al. 2008). This is a change from our previous work where we exclusively used the 2002 version of MOOG and an older grid of plane parallel MARCS models (Bell et al. 1976). We note here that the change in the version of MOOG used in our analysis necessitated an update of the log gf 's in our general line list (e.g., that used in FJP10), because they were determined differentially relative to Arcturus using MOOG and were therefore version-dependent. We have modified the log gf 's of all the lines in our general list to be correct for use with the 2010 version of MOOG and redetermined atmospheric parameters and element abundances for all the stars in our sample using the standard classical abundance techniques (see, e.g., FJP10). Changes to log gf 's were small with a mean difference of 0.01 ± 0.03 (1σ) dex and a maximum of 0.11 dex for some Ti I lines. Relevant to this current work are the stellar atmospheric parameters, Fe and Zr abundances (see below). Updated detailed abundances of other elements for these stars are available by request to the authors. Differences in atmospheric parameters and element abundances were generally small – typically within 50 K, 0.1 dex, and 0.1 km s^{-1} in T_{eff} , $\log g$ and v_t , respectively (150 K, 0.3

dex and 0.2 km s^{-1} for the most extreme cases). These differences are well within the estimated uncertainties of the original analysis (see also Section 3.3). Table 2 presents the updated atmospheric parameters and iron abundances for the stars in this work. Note that $[\text{Fe}/\text{H}]$ values are relative to a solar $\log \epsilon(\text{Fe}) = 7.52$, the default used in MOOG (see Sneden et al. 1991), and that “ σ ” denotes the (1σ) standard deviations of the Fe I and Fe II abundances.

3.2. The Neutron capture elements

We have employed both spectrum synthesis and equivalent width (EW) measurement of absorption features for the neutron-capture elements in this study. For Zr and Ba, we used EW measurements exclusively, while for La and Eu we used both EW measures and spectrum synthesis. Details of the analysis for each species are given below; here, however, we briefly summarize our methods of EW and spectrum synthesis analysis.

Measurement of line EWs is straightforward and was carried out in the same way as done for Fe and the other elements in our previous work. That is, we fit Gaussians to the line profiles interactively in IRAF (though we also measured Ba features with Voigt profiles; see below). MOOG (version 2010) was used in our spectrum synthesis analysis, in a method identical to that employed to determine oxygen abundances in our previous work. We carefully matched the resolution of the synthetic spectra

⁹ See <http://marcs.astro.uu.se/>; the models were obtained from the website 2011 July.

Table 3
Line List

Element	Wavelength (Å)	E.P.	log <i>gf</i>	log $\epsilon(X)^a$ Sun	log $\epsilon(X)^b$ Sun	log $\epsilon(X)^c$ Arcturus	[X/Fe] ^d Arcturus
Zr I	6127.48	0.150	-1.180	2.60	2.94	2.10	+0.00
Zr I	6134.55	0.000	-1.426	2.60	3.02	2.10	+0.00
Zr I	6143.20	0.070	-1.252	2.60	2.90	2.10	+0.00
Ba II	5853.70	0.604	-1.010 ^e	2.13	2.20	1.63	+0.00
Ba II	6141.70	0.704	-0.070 ^e	2.13	2.59	2.30	+0.67
Ba II	6496.90	0.604	-0.377 ^e	2.13	2.41	2.06	+0.43
La II	6262.29	0.403	-1.220 ^e	1.13	1.22	0.45	-0.18
La II	6390.48	0.320	-1.410 ^e	1.13	1.20	0.49	-0.14
Eu II	6437.64	1.319	-0.320 ^e	0.52	0.53	0.25 ^f	+0.23
Eu II	6645.10	1.379	+0.120 ^e	0.52	0.49	0.25	+0.23

^a Literature values as described in text.

^b Values found via EW measures (Zr, Ba) or spectrum synthesis (La, Eu) in this work, as described in text.

^c This study.

^d Arcturus [X/Fe] ratios calculated relative to literature solar values, adopting [Fe/H] = -0.50.

^e The total log *gf* for the feature; log *gf*'s for the individual components in La and Eu are presented in Lawler et al. (2001a) and Lawler et al. (2001b), respectively. Total log *gf*'s and those of individual components for Ba are adopted from McWilliam (1998) and Prochaska et al. (2000).

^f This abundance is forced to match that for the Eu II $\lambda 6645$ feature; see details in the text.

to the observed spectra by synthesizing absorption features of other elements near the feature of interest whose abundances we determined via EW measurement (e.g., Fe, Ca, or Ni lines). Next, we generated sets of three synthetic spectra at a time with the abundance of the element of interest varied in a stepsize 0.30 dex and the best fit abundance was determined by eye. The uncertainty in the best fit abundance was then found by decreasing the step size between the three synthetic spectra, and then varying the level of the continuum by its approximate uncertainty, until no single synthetic spectra could be identified as the best.

3.2.1. Zirconium

The zirconium abundances are based on equivalent width (EW) measurements of three Zr I lines at $\lambda 6127$, 6134, and 6143 Å. The log *gf*'s of these lines were determined by measuring their EWs in the Hinkle et al. (2000) spectrum of Arcturus and forcing the abundances to match the Zr abundance of Peterson et al. (1993; log $\epsilon(\text{Zr}) = 2.10$, normalized to the solar abundance value of Anders & Grevesse 1989, 2.60). The atomic information for these lines are given in Table 3¹⁰.

Our log *gf* values for these Zr lines are generally smaller than those found in the literature by 0.05 to 0.15 dex (e.g., Yong et al. 2005; Johnson et al. 2012). As a check on what solar abundances we would derive using these transition probabilities, we measured these lines in the solar flux atlas that accompanies the Hinkle et al. Arcturus atlas. The solar abundances we derived are shown in Table 3, and are ~ 0.30 - 0.40 dex larger than literature values (e.g., Anders & Grevesse 1989; Asplund et al. 2009; Lodders et al. 2009). This indicates that our choice of log *gf* is possibly responsible for the systematically

¹⁰ Technically, five isotopes of Zr contribute to its total abundance in solar system: ⁹⁰Zr, ⁹¹Zr, ⁹²Zr, ⁹⁴Zr, and ⁹⁶Zr (Anders & Grevesse 1989). Only odd isotopes are subject to hyperfine splitting, and as ⁹¹Zr comprises 11.22% of the solar system abundance (and therefore only a fraction of the Zr line profiles), hyperfine and isotopic splitting are not considered here.

higher Zr abundances compared to literature values for many stars in our sample, as described below, though we note that our log *gf*'s for Zr 6134 and 6143 agree within 0.1 dex of those of Johnson et al. (2012), who also found [Zr/Fe] = 0.00 for Arcturus, after adopting log $\epsilon(\text{Zr}) = 2.60$ for the Sun. Yong et al. (2005), whose log *gf*'s for these Zr lines are 0.15 dex larger than ours, found log N(Zr) = 2.80 for the Sun, and [Zr/Fe] = -0.27 for Arcturus. Smith et al. (2000), whose log *gf*'s were identical to those of Yong et al. (2005), found log N(Zr) = 2.88 for the Sun, and [Zr/Fe] = -0.24 for Arcturus. Clearly, differences in log *gf*'s do not fully account for differences in abundances here, which, in general, should be kept in mind when comparing results of different studies in the literature.

Note that for this present work, the EWs of $\lambda 6134$ and $\lambda 6143$ Å Zr I lines have been remeasured in all stars from our previous papers and therefore may be different from values published there. The abundances from the three Zr I lines are in general good agreement with abundance differences smaller than 0.1 dex for all but the lower S/N stars (e.g., NGC 2355 stars). For most of the stars from our previous work, remeasurement of $\lambda 6134$ and 6143 features, along with the addition of $\lambda 6127$ line decreased the line-by-line dispersion in abundances, and there are no systematic differences between the individual line abundances. However, for a handful of stars, the abundance from one line differed greatly from the other two; in these cases, visual inspection of the spectra and remeasurement of the EWs did not resolve the discrepancy or identify its source. In such cases, we have included lines with discrepant abundances, even though the resulting dispersion in the mean abundance is larger. Individual star [Zr/Fe] abundances, calculated relative to the [Fe I/H] ratios given in Table 2 are shown in Table 4. Mean cluster [Zr/Fe] abundances, with (1 σ) standard deviations, are shown in Table 8.

3.2.2. Barium

Table 4
Individual Star [Zr/Fe] Ratios**Table 5**
Individual Star [Ba/Fe] Ratios

Cluster	Star	Zr λ 6127 EW	Zr λ 6134 EW	Zr λ 6143 EW	[Zr/Fe] mean	[Zr/Fe] σ	Cluster	Star	Ba λ 5853 EW	Ba λ 6141 EW	Ba λ 6496 EW	[Ba/Fe] mean	[Ba/Fe] σ
Be 17	265	-0.09	-0.18	-0.10	-0.12	0.05	Be 17	265	+0.04	-0.24	+0.05	+0.04	0.01
Be 17	569	-0.15	-0.42	-0.23	-0.27	0.14	Be 17	569	+0.09	-0.23	+0.09	+0.09	0.00
Be 17	1035	+0.20	-0.14	-0.02	+0.01	0.17	Be 17	1035	+0.01	-0.16	-0.03	-0.01	0.03
Be 18	1163	+0.20	+0.04	+0.05	+0.10	0.09	Be 18	1163	+0.42	+0.11	+0.36	+0.39	0.04
Be 18	1383	+0.06	+0.02	+0.03	+0.04	0.02	Be 18	1383	+0.47	+0.16	+0.37	+0.42	0.07
Be 21	50	+0.24	+0.17	+0.17	+0.19	0.04	Be 21	50	+0.64	+0.20	+0.49	+0.56	0.11
Be 21	51	+0.10	+0.01	+0.06	+0.06	0.05	Be 21	51	+0.45	+0.26	+0.40	+0.43	0.04
Be 22	414	+0.27	+0.06	+0.10	+0.14	0.11	Be 22	414	+0.51	+0.08	+0.38	+0.45	0.09
Be 22	643	+0.80	+0.71	+0.94	+0.82	0.12	Be 22	643	+1.01	+0.41	+0.51	+0.76	0.35
Be 32	2	-0.08	+0.05	-0.01	-0.01	0.07	Be 32	2	+0.30	-0.11	+0.08	+0.19	0.16
Be 32	4	-0.14	-0.13	-0.09	-0.12	0.03	Be 32	4	+0.28	-0.14	+0.09	+0.18	0.13
Be 32	16	+0.07	+0.21	+0.18	+0.15	0.07	Be 32	16	+0.37	-0.17	+0.16	+0.27	0.15
Be 32	18	+0.21	+0.23	+0.28	+0.24	0.04	Be 32	18	+0.32	+0.01	+0.12	+0.22	0.14
Be 39	3	-0.05	-0.15	+0.08	-0.04	0.12	Be 39	3	+0.24	-0.19	+0.08	+0.16	0.11
Be 39	5	+0.07	-0.18	-0.03	-0.05	0.13	Be 39	5	+0.03	-0.55	+0.04	+0.04	0.01
Be 39	12	+0.05	+0.09	-0.05	+0.03	0.07	Be 39	12	+0.05	-0.17	+0.09	+0.07	0.03
Be 39	14	+0.16	+0.37	+0.05	+0.19	0.16	Be 39	14	-0.07	-0.16	+0.12	+0.02	0.13
M 67	105	+0.10	-0.00	+0.10	+0.07	0.06	M 67	105	+0.07	-0.31	+0.00	+0.04	0.05
M 67	141	-0.03	-0.06	-0.02	-0.04	0.02	M 67	141	+0.05	-0.30	+0.14	+0.10	0.06
M 67	170	-0.06	-0.11	+0.01	-0.05	0.06	M 67	170	+0.19	-0.17	+0.14	+0.17	0.04
N 1193	282	+0.48	+0.06	+0.45	+0.33	0.23	N 1193	282	+0.15	-0.05	+0.13	+0.14	0.01
N 1245	10	+0.20	+0.11	+0.27	+0.19	0.08	N 1245	10	+0.47	-0.08	+0.23	+0.35	0.17
N 1245	125	-0.02	+0.02	+0.22	+0.07	0.13	N 1245	125	+0.70	+0.15	+0.31	+0.51	0.28
N 1245	160	+0.54	+0.55	+0.52	+0.54	0.02	N 1245	160	+0.43	+0.20	+0.43	+0.43	0.00
N 1245	382	+0.26	+0.25	+0.29	+0.27	0.02	N 1245	382	+0.44	+0.05	+0.34	+0.39	0.07
N 1817	73	+0.34	+0.17	+0.17	+0.23	0.10	N 1817	73	+0.56	+0.15	+0.15	+0.36	0.29
N 1817	79	+0.27	-0.02	+0.11	+0.12	0.15	N 1817	79	+0.32	+0.04	+0.04	+0.18	0.20
N 188	532	+0.28	+0.06	+0.45	+0.26	0.20	N 188	532	-0.17	-0.39	-0.10	-0.14	0.05
N 188	747	+0.03	-0.07	+0.04	-0.00	0.06	N 188	747	-0.12	-0.34	+0.14	+0.01	0.18
N 188	919	+0.07	-0.27	-0.10	-0.10	0.17	N 188	919	-0.14	-0.25	+0.18	+0.02	0.23
N 188	1224	+0.13	+0.13	+0.19	+0.15	0.03	N 188	1224	+0.33	-0.07	+0.22	+0.28	0.08
N 1883	8	+0.05	-0.28	-0.15	-0.13	0.17	N 1883	8	+0.56	+0.13	+0.34	+0.45	0.16
N 1883	9	-0.01	-0.11	-0.13	-0.08	0.06	N 1883	9	+0.58	+0.20	+0.35	+0.46	0.16
N 2141	1007	-0.08	-0.04	+0.02	-0.03	0.05	N 2141	1007	+0.37	-0.01	+0.17	+0.27	0.14
N 2141	1348	+0.89	+0.45	+0.85	+0.73	0.24	N 2141	1348	+0.57	+0.33	+0.51	+0.54	0.04
N 2158	4230	-0.03	-0.10	-0.02	-0.05	0.04	N 2158	4230	+0.36	+0.04	+0.18	+0.27	0.13
N 2194	55	+0.15	+0.15	+0.29	+0.20	0.08	N 2194	55	+0.68	+0.13	+0.44	+0.56	0.17
N 2194	57	+0.17	-0.16	+0.36	+0.12	0.26	N 2194	57	+0.63	+0.20	+0.37	+0.50	0.18
N 2355	144	+0.92	...	+0.59	+0.76	0.23	N 2355	144	+0.47	+0.17	+0.46	+0.46	0.01
N 2355	398	+0.19	+0.36	+0.60	+0.38	0.21	N 2355	398	+0.90	+0.44	+0.75	+0.82	0.11
N 2355	668	+0.23	+0.47	+0.28	+0.33	0.13	N 2355	668	+0.52	+0.17	+0.40	+0.46	0.08
N 6939	121	-0.70	-0.66	-0.62	-0.66	0.04	N 6939	121	-0.16	-0.30	-0.34	-0.25	0.13
N 6939	190	+0.55	+0.48	+0.82	+0.62	0.18	N 6939	190	+0.98	+0.46	+0.60	+0.79	0.27
N 6939	212	+0.08	-0.17	-0.13	-0.07	0.13	N 6939	212	+0.38	+0.01	-0.05	+0.17	0.30
N 6939	31	+0.28	+0.11	+0.21	+0.20	0.09	N 6939	31	+0.53	+0.07	+0.04	+0.29	0.35
N 7142	196	+0.17	-0.03	+0.10	+0.08	0.10	N 7142	196	+0.19	-0.23	+0.18	+0.18	0.01
N 7142	229	+0.29	+0.04	+0.20	+0.18	0.13	N 7142	229	+0.24	-0.09	+0.21	+0.22	0.02
N 7142	377	+0.17	+0.05	+0.21	+0.14	0.08	N 7142	377	+0.21	-0.18	+0.19	+0.20	0.01
N 7142	421	+0.14	-0.10	+0.24	+0.09	0.17	N 7142	421	+0.20	-0.22	+0.16	+0.18	0.03
PWM 4	RGB 1	+0.23	+0.11	+0.22	+0.19	0.07	PWM 4	RGB 1	+0.44	+0.08	+0.24	+0.34	0.14

Note. — Individual line [Ba/Fe] ratios are calculated differentially relative to the solar Ba abundances listed in Table 3. The mean [Ba/Fe] values are calculated using the 5853 and 6496 features only. See the text for more information.

Three barium lines were measured for determination of abundances: λ 5853, 6141, and 6496Å. All three lines are quite strong and broad, and the wings of some are blended with other spectral features (namely λ 6496). Barium features are subject to both hyperfine and isotopic broadening from seven different isotopes: ^{130}Ba , ^{132}Ba , ^{134}Ba , ^{135}Ba , ^{136}Ba , ^{137}Ba , and ^{138}Ba . According to Anders & Grevesse (1989), these isotopes contribute 0.106%, 0.101%, 2.417%, 6.592%, 7.854%, 11.23%, and 71.70% of the total solar system Ba abundance, respectively. We have employed the line lists of McWilliam (1998) (see also Prochaska et al. 2000), which incorporate these isotopic fractions within the log gf's, as well as the s-process and r-process contributions to the solar system barium abundance (85% and 15%, respectively).

Abundances from these lines were calculated using

measured EWs. To determine the best method to measure EWs, we measured these lines in the Hinkle et al. (2000) Arcturus and solar flux atlases by fitting both Gaussian and Voigt profiles to them. The Ba abundances corresponding to the Gaussian line profiles are indicated in Table 3. Voigt profiles resulted in abundances 0.2-0.6 dex larger than that those for the Gaussian fits, and much more deviant from the solar value found in the literature (e.g., 2.13 – Anders & Grevesse 1989, 2.24 – Grevesse et al. 1996). We also measured Ba abundances in the Sun from these lines via spectrum synthesis and find values more consistent with the solar value: $\log \epsilon(\text{Ba}) = 2.13, 2.23, \text{ and } 2.26$ for λ 5853, 6141, and 6496, respectively. Using the same three Ba lines

Table 6
Individual Star [La/Fe] Ratios

Cluster	Star	[La/Fe] λ 6262	unc. λ 6262	[La/Fe] λ 6390	unc. λ 6390	mean[La/Fe]	σ [La/Fe]
Be 17	265	-0.33	0.30	-0.03	0.10	-0.18	0.21
Be 17	569	-0.30	0.10	-0.30	0.10	-0.30	0.00
Be 17	1035	-0.23	0.07	-0.08	0.10	-0.15	0.11
Be 18	1163	+0.16	0.05	+0.17	0.05	+0.17	0.01
Be 18	1383	+0.03	0.10	+0.18	0.06	+0.10	0.11
Be 21	50	+0.10	0.05	+0.13	0.06	+0.12	0.02
Be 21	51	+0.14	0.05	+0.17	0.05	+0.16	0.02
Be 22	414	+0.16	0.05	+0.20	0.05	+0.18	0.03
Be 22	643	+0.07	0.05	+0.36	0.07	+0.21	0.21
Be 32	2	-0.24	0.05	-0.12	0.06	-0.18	0.08
Be 32	4	-0.33	0.10	-0.18	0.07	-0.26	0.11
Be 32	16	+0.10	0.06	+0.12	0.07	+0.11	0.01
Be 32	18	+0.01	0.06	+0.03	0.06	+0.02	0.01
Be 39	3	-0.23	0.06	-0.08	0.06	-0.15	0.11
Be 39	5	-0.20	0.10	+0.02	0.06	-0.09	0.16
Be 39	12
Be 39	14	-0.06	0.10	+0.04	0.08	-0.01	0.07
M 67	105	-0.14	0.06	-0.09	0.05	-0.12	0.04
M 67	141	-0.15	0.10	-0.13	0.07	-0.14	0.01
M 67	170	-0.25	0.08	-0.15	0.09	-0.20	0.07
N 1193	282	+0.01	0.08	+0.11	0.07	+0.06	0.07
N 1245	10	-0.35	0.15	-0.30	0.10	-0.32	0.04
N 1245	125	+0.03	0.10	-0.06	0.10	-0.01	0.06
N 1245	160	+0.21	0.15	...	0.00	+0.21	0.15
N 1245	382	+0.09	0.10	+0.09	0.12	+0.09	0.00
N 1817	73	+0.10	0.10	+0.13	0.08	+0.12	0.02
N 1817	79	+0.00	0.10	+0.15	0.10	+0.07	0.11
N 188	532	+0.03	0.10	-0.10	0.10	-0.04	0.09
N 188	747	-0.19	0.10	-0.12	0.10	-0.15	0.05
N 188	919	-0.33	0.10	-0.23	0.10	-0.28	0.07
N 188	1224	+0.18	0.08	+0.30	0.12	+0.24	0.08
N 1883	8	-0.15	0.08	-0.10	0.16	-0.12	0.04
N 1883	9	+0.01	0.07	-0.01	0.10	+0.00	0.01
N 2141	1007	-0.17	0.05	-0.06	0.10	-0.12	0.08
N 2141	1348	+0.08	0.04	+0.18	0.06	+0.13	0.07
N 2158	4230	-0.16	0.07	-0.15	0.08	-0.15	0.01
N 2194	55	+0.13	0.10	+0.06	0.10	+0.10	0.05
N 2194	57	+0.00	0.08	-0.05	0.10	-0.03	0.04
N 2355	144	+0.28	0.10	+0.38	0.10	+0.33	0.07
N 2355	398	+0.07	0.08	+0.10	0.08	+0.09	0.02
N 2355	668	+0.10	0.10	+0.13	0.10	+0.12	0.02
N 6939	121	-0.41	0.10	-0.39	0.10	-0.40	0.01
N 6939	190	+0.34	0.10	+0.49	0.10	+0.42	0.11
N 6939	212	-0.19	0.08	-0.12	0.09	-0.15	0.05
N 6939	31	-0.39	0.05	-0.29	0.12	-0.34	0.07
N 7142	196	-0.24	0.10	-0.19	0.10	-0.21	0.04
N 7142	229	-0.19	0.07	-0.06	0.07	-0.12	0.09
N 7142	377	-0.21	0.07	-0.09	0.06	-0.15	0.08
N 7142	421	-0.16	0.06	-0.16	0.08	-0.16	0.00
PWM 4	RGB 1	-0.01	0.05	+0.10	0.06	+0.05	0.08

as this study, Smith et al. (2000) found $[\text{Ba}/\text{Fe}] = -0.05$ for Arcturus; Yong et al. (2005) found $[\text{Ba}/\text{Fe}] = +0.09$ based on the $\lambda 5853$ line only. Our value for $\lambda 5853$ is consistent with these values.

As a result of this analysis of the Sun and Arcturus, we measured all three Ba features in our sample stars by fitting Gaussian profiles, as these values are more consistent with those both from the spectrum synthesis analysis and from the literature. Given the especially large discrepancy between the spectrum synthesis and EW abundance for the $\lambda 6141$ line in the Sun and Arcturus, and that its abundance is also often discrepant from those of the other Ba lines in our program stars, we have opted not to include this line in the calculation of mean Ba abundances for our stellar sample, though we include it in our results for completeness. Table 5 shows the $[\text{Ba}/\text{Fe}]$ ratios for each star calculated from the in-

dividual lines, with the mean and standard deviations calculated from the $\lambda 5853$ and 6496 lines only. *Note that these $[\text{Ba}/\text{Fe}]$ ratios are calculated relative to our determined solar Ba abundances in column 6 of Table 3, to minimize systematics due to the zero-point of our abundance scale.* Mean cluster $[\text{Ba}/\text{Fe}]$ abundances, with (1σ) standard deviations, are shown in Table 8.

3.2.3. Lanthanum

^{139}La comprises 99.911% of the solar system La abundance (Anders & Grevesse 1989), and so La absorption features are subject to hyperfine broadening. We have adopted the line list of Lawler et al. (2001a), which includes data for individual hyperfine lines, for the analysis of the $\lambda 6262$ and $\lambda 6390$ Å features. We have determined La abundances for all stars in this study via both spectrum synthesis and EW measurement of the lines. We

Table 7
Individual Star [Eu/Fe] Ratios

Cluster	Star	[Eu/Fe] λ 6437	unc. λ 6437	[Eu/Fe] λ 6645	unc. λ 6645	mean [Eu/Fe]	σ [Eu/Fe]
Be 17	265	+0.02	0.12	+0.02	0.08	+0.02	0.00
Be 17	569	-0.15	0.15	-0.15	0.08	-0.15	0.00
Be 17	1035	+0.02	0.13	-0.03	0.07	-0.00	0.04
Be 18	1163	+0.11	0.15	+0.17	0.07	+0.14	0.04
Be 18	1383	...	0.00	+0.16	0.07	+0.16	0.07
Be 21	50	-0.07	0.15	-0.12	0.10	-0.10	0.04
Be 21	51	+0.14	0.08	+0.05	0.08	+0.10	0.06
Be 22	414	+0.23	0.13	+0.18	0.08	+0.21	0.04
Be 22	643	+0.41	0.08	+0.24	0.08	+0.32	0.12
Be 32	2	-0.14	0.10	-0.02	0.06	-0.08	0.08
Be 32	4	+0.00	0.08	+0.04	0.06	+0.02	0.03
Be 32	16	+0.05	0.10	+0.08	0.08	+0.07	0.02
Be 32	18	+0.13	0.07	+0.08	0.05	+0.11	0.04
Be 39	3	-0.26	0.12	-0.09	0.07	-0.17	0.12
Be 39	5	+0.00	0.13	-0.13	0.07	-0.07	0.09
Be 39	12	+0.01	0.10	-0.09	0.15	-0.04	0.07
Be 39	14	-0.01	0.13	-0.01	0.08	-0.01	0.00
M 67	105	-0.14	0.10	-0.07	0.07	-0.11	0.05
M 67	141	-0.10	0.10	-0.05	0.07	-0.08	0.04
M 67	170	-0.28	0.10	-0.13	0.07	-0.21	0.11
N 1193	282	+0.06	0.10	-0.04	0.10	+0.01	0.07
N 1245	10
N 1245	125
N 1245	160
N 1245	382
N 1817	73	-0.12	0.15	-0.07	0.10	-0.10	0.04
N 1817	79	-0.20	0.15	-0.10	0.10	-0.15	0.07
N 188	532	+0.08	0.15	-0.22	0.10	-0.07	0.21
N 188	747	-0.44	0.20	-0.04	0.12	-0.24	0.28
N 188	919	-0.53	0.20	-0.13	0.10	-0.33	0.28
N 188	1224	-0.34	0.20	+0.16	0.10	-0.09	0.35
N 1883	8	-0.30	0.13	-0.30	0.15	-0.30	0.00
N 1883	9	-0.09	0.10	-0.20	0.10	-0.15	0.08
N 2141	1007	-0.22	0.10	-0.14	0.08	-0.18	0.06
N 2141	1348	-0.22	0.10	-0.12	0.10	-0.17	0.07
N 2158	4230	-0.16	0.10	-0.11	0.10	-0.14	0.04
N 2194	55	-0.30	0.18	-0.10	0.10	-0.20	0.14
N 2194	57	-0.30	0.15	-0.30	0.15	-0.30	0.00
N 2355	144	+0.28	0.15	...	0.00	+0.28	0.15
N 2355	398	-0.01	0.10	-0.16	0.10	-0.09	0.11
N 2355	668	-0.35	0.30	-0.17	0.10	-0.26	0.13
N 6939	121	-0.31	0.15	-0.21	0.10	-0.26	0.07
N 6939	190	-0.13	0.10	-0.13	0.10
N 6939	212	-0.34	0.17	-0.11	0.08	-0.23	0.16
N 6939	31	-0.26	0.15	-0.34	0.10	-0.30	0.06
N 7142	196	-0.29	0.10	-0.19	0.10	-0.24	0.07
N 7142	229	-0.46	0.15	-0.21	0.10	-0.34	0.18
N 7142	377	-0.54	0.30	-0.19	0.10	-0.36	0.25
N 7142	421	-0.31	0.15	-0.21	0.10	-0.26	0.07
PWM 4	RGB 1	+0.07	0.10	+0.07	0.08	+0.07	0.00

take the spectrum synthesis abundance values to be more reliable, since fitting the line features with Gaussians to determine an equivalent width may not necessarily well fit the broad La features in some stars. Figure 2 shows an example spectrum synthesis of the La II 6262 feature in one of our program stars.

First though, it is useful to confirm the zero-point of our La abundances. To do so, we have determined abundances of the Sun and Arcturus via spectrum synthesis, again using the Hinkle et al. (2000) Arcturus atlas and the accompanying solar flux atlas. Using the Lawler et al. (2001a) line list, we find $\log \epsilon(\text{La}) = 1.22$ and 1.20 for $\lambda 6262$ and $\lambda 6390$ Å for the Sun, respectively (see Table 3). These values, while slightly larger than the $\log \epsilon(\text{La}) = 1.13$ found by Lawler et al. (2001a), are in good agreement with solar values found by Anders & Grevesse (1989) and meteoritic values found

by Lodders et al. (2009)¹¹. The individual line La abundances for Arcturus also agree very well (within 0.04 dex of each other); however, our mean [La/Fe] ratio for Arcturus, -0.16 ± 0.03 , is 0.10 dex lower than that found by Johnson et al. (2012) using the same line list and spectrum. Our value is even lower than that found by Yong et al. (2005) and Smith et al. (2000) for Arcturus: [La/Fe] = $+0.03 \pm 0.09$ and [La/Fe] = $+0.21$, respectively (though we note that this difference in [La/Fe] values is largely driven by a ~ 0.2 dex difference in [Fe/H] found for Arcturus between Smith et al. (2000) and other studies cited here). We adopt the Lawler et al. (2001a) solar La abundance of 1.13 to calculate [La/Fe] ratios for this

¹¹ As pointed out by the referee, Lawler et al. (2001a) used the empirical model atmosphere of the Sun from Holweger & Mueller (1974) in their analysis. This may at least partly explain the differences between our determined La abundances and their values.

Table 8
Cluster mean abundances

Cluster	[Fe/H]	σ	[Zr/Fe]	σ	[Ba/Fe]	σ	[La/Fe]	σ	[Eu/Fe]	σ	# Stars
Be 17	-0.12	0.01	-0.13	0.14	+0.04	0.05	-0.21	0.08	-0.04	0.09	3
Be 18	-0.32	0.03	+0.07	0.04	+0.41	0.02	+0.14	0.05	+0.15	0.01	2
Be 21	-0.21	0.10	+0.13	0.09	+0.50	0.09	+0.14	0.03	+0.00	0.14	2
Be 22 ¹	-0.24	0.12	+0.14	0.11	+0.45	0.09	+0.18	0.03	+0.21	0.04	1
Be 32	-0.27	0.06	+0.07	0.16	+0.22	0.04	-0.08	0.17	+0.03	0.08	4
Be 39	-0.13	0.02	+0.03	0.11	+0.07	0.06	-0.08	0.07	-0.07	0.07	4
M 67	+0.05	0.04	-0.01	0.07	+0.10	0.07	-0.15	0.04	-0.13	0.07	3
NGC 188	+0.12	0.04	+0.08	0.16	+0.04	0.17	-0.06	0.22	-0.18	0.12	4
NGC 1193	-0.17	0.13	+0.33	0.23	+0.14	0.01	+0.06	0.07	+0.01	0.07	1
NGC 1245	+0.02	0.03	+0.27	0.20	+0.42	0.07	-0.01	0.23	4
NGC 1817	-0.05	0.01	+0.18	0.08	+0.27	0.13	+0.10	0.04	-0.13	0.04	2
NGC 1883	-0.04	0.02	-0.11	0.04	+0.46	0.02	-0.06	0.08	-0.23	0.11	2
NGC 2141	-0.09	0.01	+0.50	0.71	+0.41	0.19	+0.01	0.18	-0.18	0.01	2
NGC 2158	-0.05	0.14	-0.05	0.04	+0.27	0.13	-0.15	0.01	-0.14	0.04	1
NGC 2194	-0.06	0.01	+0.16	0.06	+0.41	0.19	+0.04	0.09	-0.25	0.07	2
NGC 2355	-0.04	0.10	+0.49	0.24	+0.58	0.21	+0.18	0.13	-0.02	0.28	3
NGC 6939 ²	+0.00	0.03	-0.31	0.31	+0.07	0.28	-0.30	0.13	-0.26	0.04	3
NGC 7142	+0.08	0.02	+0.12	0.05	+0.20	0.02	-0.16	0.04	-0.30	0.06	4
PWM 4	-0.18	0.16	+0.19	0.07	+0.34	0.14	+0.05	0.08	+0.07	0.01	1

¹ [X/Fe] ratios calculated without star 643.

² [X/Fe] ratios calculated without star 190.

study. Individual star [La/Fe] ratios as determined via spectrum synthesis are shown in Table 6. The abundance uncertainty for each line given in this Table represents the measurement uncertainty in the synthesis technique, as described in the introduction of this Section. Mean cluster [La/Fe] abundances, with (1 σ) standard deviations, are shown in Table 8. (For cluster abundances based on the measures of a single star only, the 1 σ value represents the uncertainty (standard deviation) in its abundance from Table 6.)

Abundances from each La II feature were also determined using measured EWs and the *blends* driver in MOOG, to correctly account for the hyperfine structure of the lines. Differences between synthesis and EW abundances for each line were plotted against [Fe/H], T_{eff} , and log g to look for systematic trends. For the 6262 feature, the EW abundances were ~ 0.07 smaller than the synthesis abundances, with a standard deviation of ~ 0.15 dex. While no trend with [Fe/H] is present, the difference between EW and synthesis abundances grows larger (that is, EW abundances get increasingly smaller relative to the synthesis values) with increasing T_{eff} and log g . For the 6390 feature, the difference between EW and synthesis abundances (in the sense EW – synthesis) is $\sim +0.13$, with a standard deviation of ~ 0.12 dex. No trend is present versus [Fe/H], T_{eff} , or log g .

3.2.4. Europium

Like lanthanum, europium is subject to strong hyperfine splitting. However, while La features are predominantly composed of a single isotope, Eu features are also subject to splitting between two isotopes. We have adopted the line list for the Eu II $\lambda 6437$ and $\lambda 6645$ Å features from Lawler et al. (2001b), assuming the standard solar system isotopic mix of 47.8% ¹⁵¹Eu and 52.2% ¹⁵³Eu (Anders & Grevesse 1989).

It is important to state that, according to Lawler et al. (2001b), the $\lambda 6437$ Å feature is significantly blended with a silicon feature at $\lambda 6437.71$ Å. We have attempted to reduce the impact of this blend and recover reliable Eu

abundances from this feature in the following way. We measured the Eu abundance for Arcturus from the Eu II $\lambda 6645$ line and set that as the “true” Eu abundance: $\log \epsilon(\text{Eu}) = 0.25$. We then generated a synthetic spectrum of the $\lambda 6437$ feature using Arcturus’s atmospheric parameters, the Eu abundance from the $\lambda 6645$ line, and the Si abundance we have adopted for Arcturus (and which served as the basis for our astrophysical log gf ’s; we also used an E.P. of 5.863 eV, retrieved from VALD¹²). We then altered the log gf of the $\lambda 6437.71$ Si feature until the synthetic spectrum matched the Arcturus spectrum, and used this log gf (-2.30) for the Si feature in the synthesis line list for Eu $\lambda 6437$. Lastly, in the spectrum synthesis analysis of our sample stars, we set the Si abundance of this blend feature to match that for each star as determined from the EW analysis of other Si lines in its spectrum.

As for La, we verified our method of analysis with the Sun. Spectrum synthesis using the solar flux atlas from Hinkle et al. (2000) resulted in $\log \epsilon(\text{Eu}) = 0.53$ and 0.49 for $\lambda 6437$ and $\lambda 6645$, respectively. These values are consistent to those found by Lawler et al. (2001b) for the same lines: 0.55 and 0.54. For Arcturus, our [Eu/Fe] = +0.23 is in good agreement with that found by Johnson et al. (2012) and Yong et al. (2005), again using similar analysis techniques ([Eu/Fe] = +0.29 in both studies, from only the $\lambda 6645$ line). Our value of [Eu/H] = -0.27 for Arcturus is also in good agreement with Smith et al. (2000), who found [Eu/H] = -0.30 . Table 7 presents the [Eu/Fe] ratios for our sample as determined from spectrum synthesis. Again, the abundance uncertainties associated with each line represents the measurement uncertainty from the synthesis technique. We note that the S/N ratios of the spectra of all four NGC 1245 stars were too low to determine reliable abundances for the relatively weak (< 20 mÅ in these stars) Eu II features. Mean cluster [Eu/Fe] abundances,

¹² See <http://vald.astro.univie.ac.at/~vald/php/vald.php>, Kupka et al. (2000).

Table 9
Uncertainties in abundance ratios due to atmospheric parameters

Star	El.	T+100 K Δ abund.	log g+0.2 dex Δ abund.	[M/H]+0.2 dex Δ abund.	v_t +0.2 km s ⁻¹ Δ abund.
N6939 31	[Fe/H]	-0.03	+0.06	+0.05	-0.13
	[Zr/Fe]	+0.19	-0.01	+0.01	-0.09
	[Ba/Fe] ₅₈₅₃	+0.03	+0.01	+0.06	-0.09
	[Ba/Fe] ₆₄₉₆	+0.04	+0.01	+0.06	-0.03
	[La/Fe] ₆₂₆₂	+0.05	+0.06	-0.06	+0.13
	[La/Fe] ₆₃₉₀	+0.00	+0.10	-0.17	+0.11
	[Eu/Fe] ₆₄₃₇	-0.02	+0.05	-0.09	+0.01
	[Eu/Fe] ₆₆₄₅	+0.02	+0.03	+0.02	+0.12
N1817 79	[Fe/H]	+0.09	+0.01	+0.01	-0.07
	[Zr/Fe]	+0.06	-0.01	-0.01	+0.07
	[Ba/Fe] ₅₈₅₃	-0.07	+0.06	+0.04	-0.15
	[Ba/Fe] ₆₄₉₆	-0.06	+0.05	+0.06	-0.13
	[La/Fe] ₆₂₆₂	-0.06	+0.08	-0.01	+0.06
	[La/Fe] ₆₃₉₀	-0.03	+0.09	-0.04	+0.07
	[Eu/Fe] ₆₄₃₇	-0.08	+0.10	-0.25	+0.14
	[Eu/Fe] ₆₆₄₅	-0.10	+0.08	+0.05	+0.06
N1883 9	[Fe/H]	+0.06	+0.03	+0.02	-0.10
	[Zr/Fe]	+0.14	-0.02	-0.03	+0.08
	[Ba/Fe] ₅₈₅₃	-0.06	+0.05	+0.06	-0.14
	[Ba/Fe] ₆₄₉₆	-0.04	+0.04	+0.06	-0.07
	[La/Fe] ₆₂₆₂	-0.04	+0.07	+0.00	+0.09
	[La/Fe] ₆₃₉₀	+0.00	+0.11	-0.11	+0.09
	[Eu/Fe] ₆₄₃₇	-0.08	+0.08	-0.11	+0.09
	[Eu/Fe] ₆₆₄₅	-0.07	+0.07	+0.05	+0.09
N7142 196	[Fe/H]	+0.03	+0.04	+0.04	-0.10
	[Zr/Fe]	+0.18	-0.03	-0.05	+0.04
	[Ba/Fe] ₅₈₅₃	-0.01	+0.03	+0.03	-0.15
	[Ba/Fe] ₆₄₉₆	-0.01	+0.01	+0.06	-0.06
	[La/Fe] ₆₂₆₂	-0.01	+0.07	-0.07	+0.10
	[La/Fe] ₆₃₉₀	-0.02	+0.09	-0.10	+0.09
	[Eu/Fe] ₆₄₃₇	-0.06	+0.08	-0.12	+0.06
	[Eu/Fe] ₆₆₄₅	-0.05	+0.04	+0.02	+0.09
PWM 4 1	[Fe/H]	-0.03	+0.05	+0.03	-0.13
	[Zr/Fe]	+0.20	+0.00	-0.01	-0.06
	[Ba/Fe] ₅₈₅₃	+0.04	+0.02	+0.04	-0.07
	[Ba/Fe] ₆₄₉₆	+0.04	+0.01	+0.04	-0.02
	[La/Fe] ₆₂₆₂	+0.05	+0.05	+0.00	+0.13
	[La/Fe] ₆₃₉₀	+0.02	+0.07	-0.08	+0.10
	[Eu/Fe] ₆₄₃₇	-0.01	+0.05	-0.03	-0.01
	[Eu/Fe] ₆₆₄₅	+0.01	+0.04	+0.02	+0.11
Be 22 414	[Fe/H]	+0.03	+0.04	+0.03	-0.10
	[Zr/Fe]	+0.16	-0.03	-0.05	+0.03
	[Ba/Fe] ₅₈₅₃	-0.01	+0.02	+0.02	-0.15
	[Ba/Fe] ₆₄₉₆	+0.00	+0.00	+0.04	-0.05
	[La/Fe] ₆₂₆₂	-0.01	+0.05	-0.02	+0.10
	[La/Fe] ₆₃₉₀	-0.01	+0.07	-0.10	+0.09
	[Eu/Fe] ₆₄₃₇	-0.05	+0.06	-0.04	+0.05
	[Eu/Fe] ₆₆₄₅	-0.04	+0.05	+0.02	+0.09

with (1 σ) standard deviations, are shown in Table 8. (As for La, the 1 σ value for clusters based on the analysis of a single star represents the uncertainty (standard deviation) in its abundance from Table 7.) The bottom panel of Figure 2 shows an example synthesis of the Eu II 6645 feature.

It can be seen in Table 7 that the Eu abundances determined from the λ 6437 feature generally agree well (i.e. with differences comparable to or smaller than the measurement uncertainties) with that of the λ 6645 feature for most stars. However, larger discrepancies are evident for some stars, especially those in clusters NGC 188 and NGC 7142. While differing line abundances could be due to uncertainties in continuum placement or less-than-optimal S/N ratios for some stars, the stars exhibiting the largest abundance discrepancies are generally the more metal rich stars in the sample, with [Fe/H] values

of \sim 0.10 or higher. For such metal-rich stars, our fix for neutralizing the Si blend in the λ 6437 feature may break down.

Eu abundances were determined using measured EWs and the *blends* driver in MOOG, similar to lanthanum. As before, differences between EW and synthesis abundances were plotted against stellar [Fe/H], T_{eff} and log g. Both Eu features show a trend of increasing difference with increasing [Fe/H], but no trend with T_{eff} or log g (maybe a slight trend with log g for λ 6437). The mean difference for both lines is \sim 0.1 dex, with the smallest abundance difference for metal poor stars (\sim 0 dex) and the largest abundance difference (\sim 0.2 dex) for the more metal-rich.

Table 10
Cluster abundances from the literature

Cluster	Ref	[Zr/Fe]	[Ba/Fe]	[La/Fe]	[Eu/Fe]	Notes
Be 18	Yong et al. (2012)	-0.21±0.13	+0.30±0.06	+0.34±0.08	+0.30±0.06	2 stars
Be 21	Yong et al. (2012)	-0.11±0.08	+0.59±0.01	+0.56±0.01	+0.31±0.08	2 stars
Be 22	Yong et al. (2012)	-0.14	+0.61±0.05	+0.38±0.02	+0.26±0.10	2 stars
Be 32	Yong et al. (2012)	-0.06±0.07	+0.29±0.12	+0.44±0.02	+0.31±0.11	2 stars
Be 32	D’Orazi et al. (2009)	...	+0.24±0.15	9 stars
Be 32	Carrera & Pancino (2011)	...	+0.51±0.12	-0.14±0.07	...	2 stars
M 67	Yong et al. (2005)	-0.28±0.03	-0.02±0.04	+0.11±0.02	+0.06±0.03	3 stars
M 67	Tautvaišienė et al. (2000)	-0.17±0.09	+0.07±0.09	+0.13±0.09	+0.07±0.09	9 stars
M 67	D’Orazi et al. (2009)	...	+0.04±0.05	10 stars
M 67	Maiorca et al. (2011)	+0.04±0.05	...	+0.06±0.04	...	10 stars
M 67	Pancino et al. (2010)	...	+0.25±0.06	+0.05±0.06	...	3 stars
NGC 1817	Reddy et al. (2012)	+0.08±0.05	+0.13	+0.12±0.03	+0.13	3 stars
NGC 2141	Yong et al. (2005)	+0.63±0.06	+0.91	+0.57±0.07	+0.17	1 star
PWM 4	Yong et al. (2012)	+0.11±0.06	+0.46	+0.22±0.07	+0.12	1 star

As in our previous work, we estimate the uncertainties in atmospheric parameters to be 100 K in T_{eff} , 0.2 dex in $\log g$, and 0.2 km s $^{-1}$ in microturbulent velocity. We have calculated uncertainties in [Fe/H] and [X/Fe] ratios due to these uncertainties in atmospheric parameters for six stars in our sample that span a wide range in atmospheric parameters and metallicities. The results are presented in Table 9. We did not consider the covariance terms in the error analysis, rather we treated the uncertainty in each parameter as though they were independent of one another. The uncertainty calculations for La and Eu lines were performed using EWs, not spectrum synthesis. We include here also the abundance changes due to an uncertainty of 0.2 dex in the model atmosphere [M/H] value. This is meant to be indicative only of the impact that such an uncertainty would have; given that we always matched the [M/H] of the model to the iron abundance of each star, this uncertainty is overly conservative. As can be seen, [X/Fe] uncertainties are generally smaller than 0.10 dex, but occasionally as large as 0.20 dex.

To estimate the uncertainty in the Eu abundance calculated from the $\lambda 6437$ line due to the Si blend, we generated a synthetic spectrum for each of the stars in Table 9 with the Si abundance varied by the line-by-line dispersion in its Si abundance as measured from EWs of Si lines. The best fit Eu abundance was then compared to the abundances given in Table 7. Line-by-line dispersions in Si abundances ranged from 0.08 to 0.16 dex. Corresponding changes in the Eu abundance ranged from 0 to ~ 0.15 dex, with a median change of only 0.02 dex.

3.4. Anomalous stars

A few clusters contain stars that exhibit strikingly different n-capture abundance patterns.

Be 22: Star 643 is much more enhanced in [Zr/Fe] and [Ba/Fe] than star 414. In fact, the abundances of several other elements in 643 differ significantly from those of 414, and the general line-by-line dispersion in element abundances is also higher (even for iron; we also note that Y12 found similar behavior). Given that 643 is high up on the red giant branch relative to 414 (e.g., Figures 5 & 6 in Y12), we have taken the abundances of star 414 to be more reliable, and therefore we have adopted the abundances of star 414 as representative of those for Be 22 as a whole. The abundances reported for Be 22 in

Table 8 are exactly those of star 414.

NGC 2141: Star 1348 shows systematically larger enhancements in [Zr/Fe], [Ba/Fe] and [La/Fe] than star 1007, though their [Eu/Fe] ratios are nicely consistent (see Figure 1). They have very similar atmospheric parameters, metallicity, and other element abundances. We also note that Yong et al. (2005) also found high [Zr/Fe], [Ba/Fe], and [La/Fe] ratios for star 1348. Given the similar evolutionary states of these two stars, we do not choose one and exclude the other as we have done for Be 22. Instead, we have averaged the abundances of the two stars together, and therefore the mean abundances of this cluster show large dispersions in the subsequent discussion.

NGC 6939: Stars in this cluster show a pattern in which one star, 190, is consistently enhanced in [X/Fe] ratios, and another (121) is consistently under-abundant relative to the remaining two stars. Star 190 resides in the clump and shows [s/Fe] ratios at least 0.4 dex larger than the other stars. As a result we do not include it in cluster mean abundance calculations. Star 121 is more of a puzzle, as it is not systematically different from the other two cluster members for the other elements. However, we note that the spectroscopic T_{eff} that we found by minimizing Fe I abundances versus line E.P. is 300 K cooler than the photometric T_{eff} (Jacobson et al., in prep.), while the photometric and spectroscopic temperatures for the other stars agree within 50 K. Therefore, it is possible that star 121’s discrepant [X/Fe] ratios are due to offsets in its atmospheric parameters.

Other stars show less pathological differences from their counterparts. For example, star 398 in NGC 2355 is 0.3 dex more enhanced in [Ba/Fe], while star 1224 in NGC 188 also shows larger (~ 0.2 -0.3 dex) enhancements in [Ba/Fe] and [La/Fe] than the other NGC 188 stars, even after taking into account line-to-line abundance dispersions. The four stars in NGC 1245 show large variations in [La/Fe], but this may be the result of relatively low S/N ratios for the spectra (indeed, they were deemed too poor to reliably measure Eu abundances). In general, star-to-star variations in abundances of the r-process element Eu are much smaller than for the s-process elements. For example, the pairs of stars in Be 22 and NGC 2141 that differ in [s/Fe] ratios have similar [Eu/Fe] ratios, and the Eu abundance for star 190 in NGC 6939 is consistent within the uncertainties of the other stars

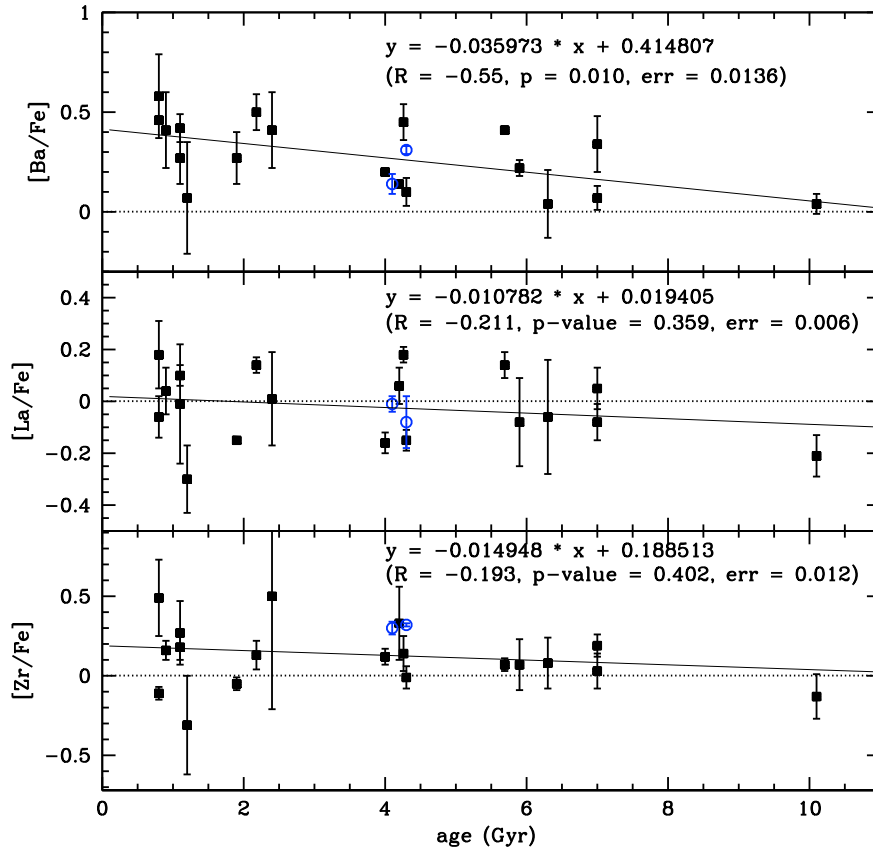


Figure 3. [Ba/Fe] (top panel), [La/Fe] (middle panel), and [Zr/Fe] (bottom panel) ratios for our cluster sample (filled squares) as a function of cluster age. The open blue circles represent clusters Be 20 and Be 29 from Yong et al. (2005) shifted on to our abundance scale (see text for details). The equations for least squares fits to the data are indicated in all panels, along with the R-values, p-values, and errors of the fit.

in the cluster. Instead, the two stars in Be 21 differ in [Eu/Fe] by 0.2 dex, but at a $2\text{-}\sigma$ level. Not surprisingly, the star-to-star scatter is larger for NGC 188 and NGC 2355 stars, with standard deviations in [Eu/Fe] of 0.12 and 0.28 dex, respectively.

3.5. Comparison to other studies

To our knowledge, abundances of neutron capture elements are available in the literature for eight clusters in our study. Table 10 gives a summary of these literature results. Not surprisingly, M 67 is the most well-studied with two sets of measures for Zr, Ba, La, and Eu (Yong et al. 2005; Tautvaišienė et al. 2000), and three additional studies of Ba and La abundances (D09; M11; Pancino et al. 2010). For this cluster, our [Ba/Fe] ratio is consistent with the roughly scaled-solar values found by these studies, save for the $[\text{Ba}/\text{Fe}] = +0.25 \pm 0.06$ value found by Pancino et al. (2010). Our [La/Fe] ratio of -0.15 ± 0.04 for M 67 is systematically lower than those of other studies, which found $[\text{La}/\text{Fe}] \sim 0.05$ to 0.13 dex. Our [Eu/Fe] measures for M 67 stars are also lower than the findings of other studies in the literature (e.g., $+0.07 \pm 0.09$ – Tautvaišienė et al. 2000, $+0.06 \pm 0.03$ – Yong et al. 2005). As for Zr, our value is consistent with that of M11, but is larger than those values found by Yong et al. and Tautvaišienė et al.

The next best-studied cluster is Be 32, with lit-

erature abundances again from Y12, D09, M11, and Carrera & Pancino (2011). As for M 67, our mean cluster [Ba/Fe] ratio agrees well with those of Y12 and D09 (within 0.05 dex), but is ~ 0.25 dex lower than that of Carrera & Pancino. Only Carrera & Pancino and Y12 presented [La/Fe] ratios for Be 32; our value is in good agreement with the former (within 0.06 dex), but is lower than the latter by 0.5 dex! Similarly our [Eu/Fe] ratio is 0.3 dex lower than that of Y12, but our scaled-solar [Zr/Fe] is consistent with their findings.

The recent work by Reddy et al. (2012) also presented neutron capture abundances for NGC 1817. Here we find consistent [La/Fe] ratios (within 0.02 dex) for the cluster, while our [Ba/Fe] and [Zr/Fe] ratios are consistent within the uncertainties. Our Eu abundances, however, are very different: their $[\text{Eu}/\text{Fe}] = +0.13$ is 0.26 dex larger than our value.

In addition to the clusters mentioned above, clusters NGC 2141, Be 18, Be 21, Be 22 and PWM 4 are in common with Yong et al. (2005, 2012) – recall the stars and spectra for the three Berkeley clusters and star 1348 in NGC 2141 are those of Yong et al., and we have in addition two M 67 stars in common (105 and 141). A star by star comparison of the 12 stars common between our two samples shows that differences between our abundances (in the sense This Study – Yong) for [Ba/Fe], [La/Fe], [Eu/Fe] and [Zr/Fe] are $+0.04 \pm 0.19$,

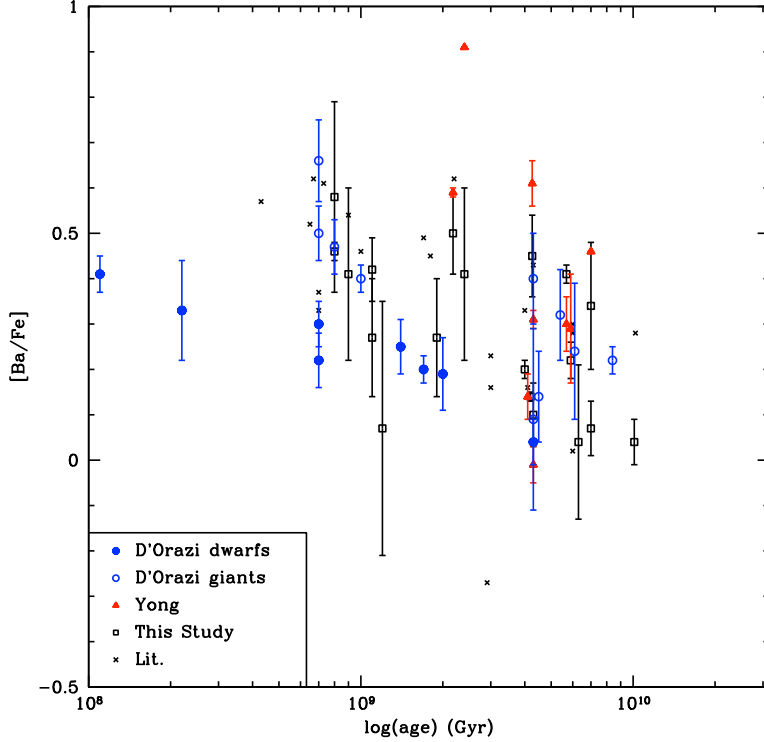


Figure 4. $[\text{Ba}/\text{Fe}]$ versus $\log(\text{age})$ for our clusters (open squares), those of Yong et al. (2005, 2012; red triangles), and the sample of D09 (dwarfs – filled blue circles, giants – open blue circles). Other clusters from the literature are represented by small crosses. See text for more information.

-0.29 ± 0.12 , -0.16 ± 0.13 , and $+0.26 \pm 0.10$ dex, respectively. The standard deviations of this difference for La, Eu, and Zr are comparable to individual star uncertainties, while the scatter for Ba is larger, indicating that the differences between our studies are systematic for La, Eu and Zr, but not for Ba. For the discussions that follow, we have made use of these systematic differences to place two additional clusters studied by Yong et al. (2005), Be 20 and Be 29, on to our cluster abundance scale.

4. DISCUSSION

In order to minimize possible systematic uncertainties in the cluster abundance results as much as possible, we limit our discussion to the results of this work with the addition of Be 20 and Be 29 from Yong et al. (2005), as just discussed. For the first discussion, that of abundance trends with age and R_{gc} , our sample size is comparable to those of D09 and M11 and yet is almost completely distinct from them, with only two clusters in common to each (M 67 and Be 32). Therefore, this dataset provides an excellent opportunity to look for the anticorrelation of cluster s-process abundance ($[\text{s}/\text{Fe}]$) with cluster age found by D09 and M11, and further explored in, Maiorca et al. (2012).

4.1. Cluster *n*-capture abundance trends with age

The first s-process element shown to have enhancements anti-correlated with open cluster age was barium (D09), so we begin with it here. The top panel of Figure 3 shows mean cluster $[\text{Ba}/\text{Fe}]$ ratios from Table 8 plotted against cluster age (taken from Salaris et al. 2004). In this figure, our sample is represented with squares,

while open blue circles represent the outer disk clusters Be 20 and Be 29 from Yong et al. (2005), shifted to our abundance scale. A simple linear regression analysis on the distribution of the points resulted in the equations for lines of best fit through the data also printed in each panel. Also included are the R-value, standard error of the estimate for regression (err; i.e., the degree of scatter of the points around the regression line), and the two-tailed probability estimate (p-value), a measure of the statistical significance of the slope. Conventionally, p-values smaller than 0.05 or 0.01 are taken to be rejections of the null hypothesis, which in this case is that there is no trend in $[\text{X}/\text{Fe}]$ ratio with cluster age. As can be seen in Figure 3, our data do show a statistically significant trend of increasing $[\text{Ba}/\text{Fe}]$ with decreasing cluster age, as shown in the sample of D09. If the oldest cluster, Be 17, is excluded, the p-value increases from $p=0.010$ to $p=0.048$, decreasing the significance of the trend.

Results from our sample also agree with those of Y12, who found a similar slope of $[\text{Ba}/\text{Fe}]$ with age, of -0.03 ± 0.01 , from their sample of 10 clusters combined with another 22 measurements taken from the literature. As they note, this trend is not as pronounced as that found in D'Orazi et al. The advantage of the work presented here is that it includes 3 more clusters with ages greater than 6 Gyr. Notably, our $[\text{Ba}/\text{Fe}]$ ratios for these old clusters are all roughly solar, reinforcing the significance of the trend of decreasing Ba with cluster age. Nevertheless, the correlation shows substantial scatter about the mean trend. This can also be seen in Figure 4, which replicates Figure 1 in D09 (open and filled blue circles), with our sample (open squares) also included. Here, we

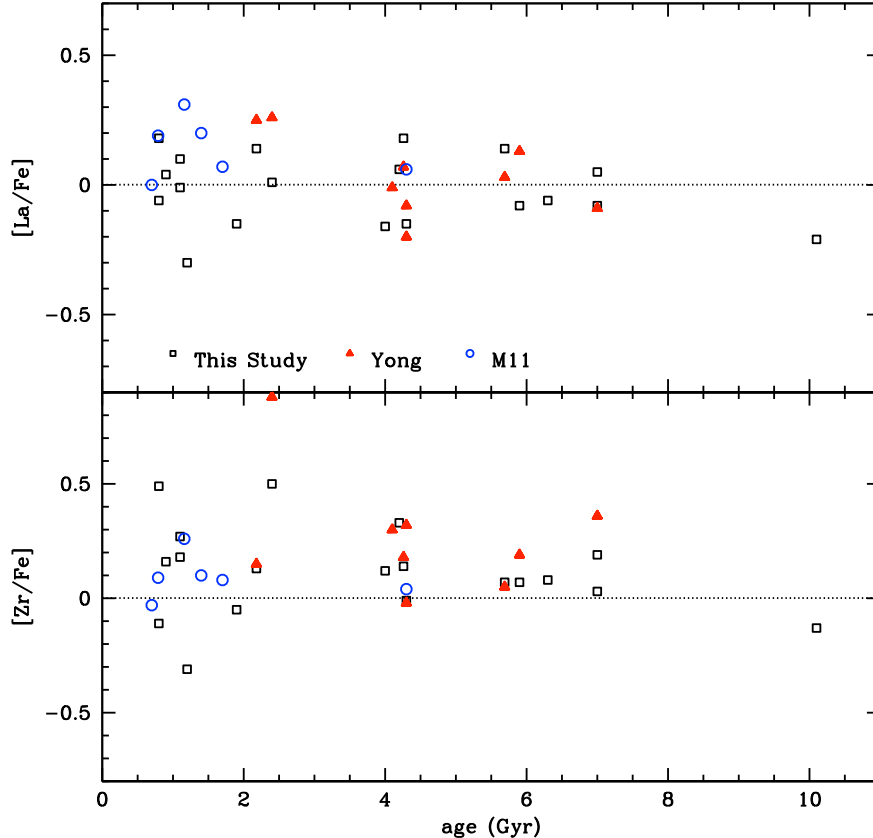


Figure 5. $[La/Fe]$ (top) and $[Zr/Fe]$ (bottom) abundance ratios versus age for our sample (open squares), those of Yong et al. (2005, 2012; red triangles) shifted to our abundance scale, and those of M11 (blue open circles). Error bars have been omitted for clarity. As described in the text, the $[s/Fe]$ for clusters from M11 fit nicely within the distribution of our sample.

include the full cluster sample of Yong et al. (2005, 2012; red triangles), along with clusters from the literature as compiled in Y12 (their Table 13) represented by small crosses. We follow Y12 here in that we treat each measure of an individual cluster independently, and therefore some clusters are represented by multiple points in this figure. It can be seen that although each sample spans a slightly different range in age, they follow the same general trend of increasing $[Ba/Fe]$ with decreasing age. This is even seen in the inhomogeneous cluster sample drawn from the literature.

The middle panel of Figure 3 shows cluster $[La/Fe]$ versus age for our sample, again with two outer disk clusters from Yong et al. (2005) adjusted to our abundance scale. M11 found a trend of increasing $[La/Fe]$ with decreasing cluster age, but this was based on only six clusters in their sample for which they could determine La abundances (the trend of $[s/Fe]$ with cluster age is much more convincing for the s-process elements Ce and Y, for which they have abundances for all 19 clusters in their sample). We note that the clusters for which they determined La abundances covered a much more limited age range (and a primarily younger one) than that presented here. The larger sample of Figure 3 clearly shows no trend of $[La/Fe]$ with cluster age: the p-value is quite large. Indeed, while Be 17 shows a subsolar $[La/Fe]$ ratio that drives some slope to the data, the rest of the clusters

show an essentially flat distribution, again with a scatter of roughly 0.3 dex.

Y12, on the contrary, found a positive correlation of $[La/Fe]$ with age, with a slope of 0.05 ± 0.01 , based on their determinations for 10 clusters and literature values for 6 more. However, recall that our values of $[La/Fe]$ for stars in common to the Y12 analysis showed a systematic offset of 0.29 dex, ours being lower. When the Y12 values are adjusted to our abundance scale, the trend with age disappears entirely, yielding results consistent with ours, as can be seen in the top panel of Figure 5. Here, the sample of Y12, shifted to our abundance scale, is indicated by red triangles, while the six clusters in M11 are blue circles. We conclude that none of the available data from these larger samples (that is, ours and Y12) show evidence for age trends in La abundance, once systematic differences are taken into account, and the distribution with age of the M11 sample is consistent with this observation.

M11 also claimed a trend in their cluster $[Zr/Fe]$ ratios versus cluster age, but as for La this was based on a subset of their sample of only 6 primarily younger clusters. We see no trend in our cluster $[Zr/Fe]$ ratios versus age; indeed, the distribution is very similar to that of $[La/Fe]$ (bottom panel of Figure 3). Interestingly, the dispersion of $[Zr/Fe]$ ratios with age is fairly tight at 0.1-0.2 dex for clusters around 6-7 Gyr of age, with the dispersion in-

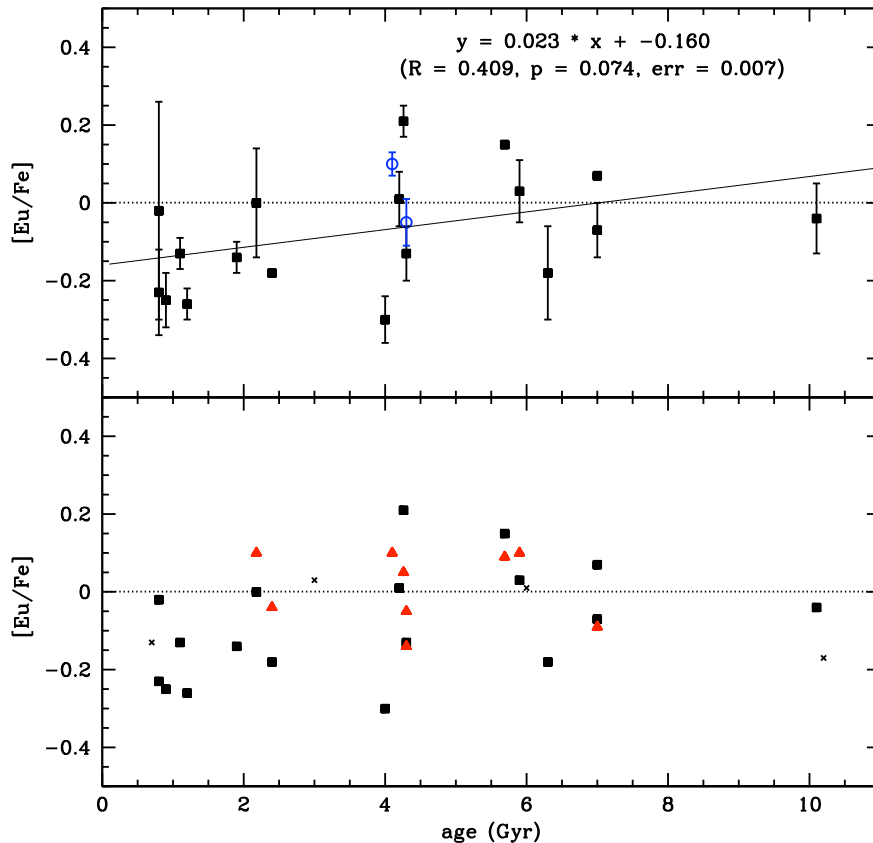


Figure 6. Top panel: $[\text{Eu}/\text{Fe}]$ versus age; symbols same as in Figure 3. Bottom panel: $[\text{Eu}/\text{Fe}]$ for our cluster sample (filled squares), along with those of Yong et al. (2005, 2012; red triangles) shifted to our abundance scale, and other clusters from the literature (crosses).

creasing with decreasing cluster age. We note the cluster with $[\text{Ba}/\text{Fe}] \sim 0.70$ with the huge errorbars is NGC 2141, whose large and discrepant Zr abundances have already been discussed.

Y12 also found a slight anticorrelation of $[\text{Zr}/\text{Fe}]$ with cluster age, with a slope of -0.03 ± 0.01 , based again on their sample plus results from the literature, the majority of which were taken from our previous papers. We note that these earlier Zr abundances have been revised and updated in this paper, as discussed in Section 3. Y12 also noted that the trend of Zr with age was more moderate than that cited by M11. However, as with La, the $[\text{Zr}/\text{Fe}]$ abundances for the M11 sample are consistent with the distribution of points shown in the bottom panel of Figure 5, and support the conclusion that there is no trend of $[\text{Zr}/\text{Fe}]$ abundances with age among the open clusters from this larger sample.

Few determinations of Eu exist for stars in open clusters, yet the behavior of this r-process element relative to the s-process elements we have considered thus far is especially interesting. Figure 6 shows cluster $[\text{Eu}/\text{Fe}]$ trends versus age for our sample. Our data show a trend of *increasing* $[\text{Eu}/\text{Fe}]$ with *increasing* cluster age but only at a marginally statistically significant level. What is more notable in these figures is how the dispersion in cluster $[\text{Eu}/\text{Fe}]$ ratio varies with age: for example, the dispersion in $[\text{Eu}/\text{Fe}]$ among 4 Gyr old clusters spans nearly 0.6 dex, while the dispersion of the older and

younger clusters is 0.3-0.4 dex. Clearly, this could just be a result of the small size of our cluster sample, but it would be interesting to see if these dispersions hold in larger homogeneous cluster studies. Y12 found no trend of $[\text{Eu}/\text{Fe}]$ with age in their analysis, based on their results for 10 clusters plus four others from the literature. Those results are consistent with our larger sample, as can be seen in the bottom panel of Figure 6.

As mentioned in the introduction, da Silva et al. (2012) found trends of increasing $[\text{s}/\text{Fe}]$ with decreasing age for dwarf stars in the solar neighborhood, most notably for Ba, but also for Zr, Y and Ce. Of these elements, only Y shows this anticorrelation across the full age range of their sample; the anticorrelation is present for the other elements only for the stars younger than the Sun (4.5 Gyr). They argue, as D09 and M11 do, that this indicates that the s-process yields of AGB stars has changed over time (as well as $[\text{Fe}/\text{H}]$ of the AGB stars), and the fact that Ba shows the strongest trend with age implies that this change in yields affects the heavy s-process elements more than it does the light ones. While we find the consistency between the results of da Silva et al. (2012) and D09/M11 compelling, we would argue that the $[\text{La}/\text{Fe}]$ trends seen in Figures 3 and 5 of this work may indicate that the source of an $[\text{s}/\text{Fe}]$ abundance trend with age does not affect all heavy s-process elements equally.

Indeed, the picture becomes more complicated when

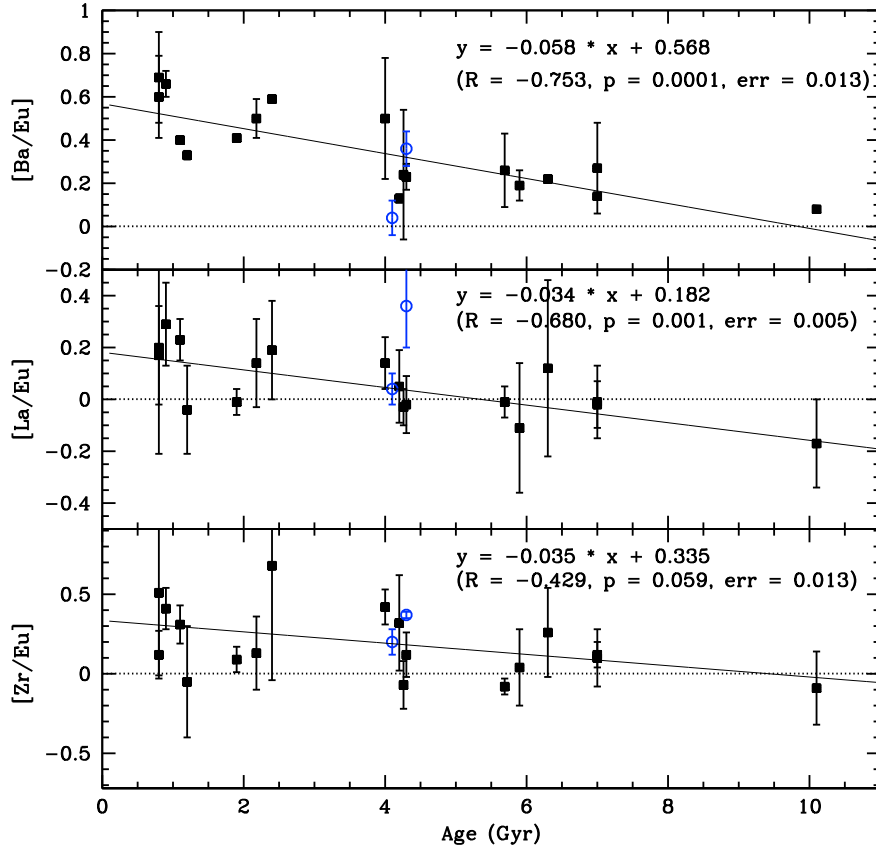


Figure 7. [Ba/Eu] (top panel), [La/Eu] (middle panel), and [Zr/Eu] (bottom panel) versus age. Symbols are the same as in Figure 3.

other (larger) solar neighborhood dwarf star studies are considered. We performed a regression analysis of [X/Fe] versus age for solar neighborhood (thin disk) dwarf stars from the studies of Reddy et al. (2003) and Bensby et al. (2005), considering the full age range of their samples as well as stars 4.5 Gyr or younger. For the Reddy et al. (2003) sample, [Zr/Fe] showed a statistically significant trend with decreasing stellar age for both age ranges considered, while [Nd/Fe]¹³ showed a statistically significant trend with (increasing) age only when the full age range the sample was considered. For the Bensby et al. (2005) sample, only [Ba/Fe] showed a statistically significant trend with (decreasing) age, for both age ranges considered. None of the other s-process species studied by these two groups (Y for Bensby et al. 2005; Ba and Ce for Reddy et al. 2003) showed trends with age. (The lack of a trend of [Ba/Fe] with decreasing cluster age for the Reddy et al. (2003) sample may be due to the fact that that sample contained very few stars with young (<1-2 Gyr) ages. If the distribution of [Ba/Fe] ratios with age is non-linear, and in fact only becomes steeply anti-correlated with age for the youngest objects (e.g., the youngest clusters in D09), then such a trend would not appear in a sample of older stars.)

Regarding r-process abundance trends with age, da Silva et al. (2012) did not determine Eu abundances

for their sample. However, they did report abundances for Sm, which is also representative of the r-process. They also reported a trend of increasing [Sm/Fe] with increasing age for their sample, consistent with the Eu results for our open cluster sample. The Reddy et al. (2003) sample also showed statistically significant trends of [Eu/Fe] with increasing stellar age, but the Bensby et al. (2005) sample did not.

In Figure 7 we explore trends of [X/Eu] ratios versus age for Ba, La and Zr individually. Trends of increasing [Ba/Eu] and [La/Eu] with decreasing cluster age can be seen, while that for [Zr/Eu] is less convincing. These trends are consistent with the [s/Sm] versus age trends in da Silva et al. (2012), although the trends in their sample are especially pronounced for stars younger than the Sun. We interpret this as evidence of the increasing importance/efficiency of s-process enrichment relative to the r-process in the Milky Way thin disk over time.

This analysis did not take into account uncertainties in the ages of the clusters, which can sometimes be significant. We have chosen to use the cluster ages as determined in Salaris et al. (2004) which rest on a calibration of the morphological age indicator of Janes & Phelps (1994). While this method may not be as accurate for any given cluster as direct fitting of isochrones to cluster color magnitude diagrams, it has the advantage of placing all the cluster ages on a uniform relative scale. The typical age uncertainty of the Salaris et al. calibration is 15%, which for our clusters is less than 1 Gyr.

¹³ Technically, Nd is ~50% s-process and ~50% r-process (Burriss et al. 2000).

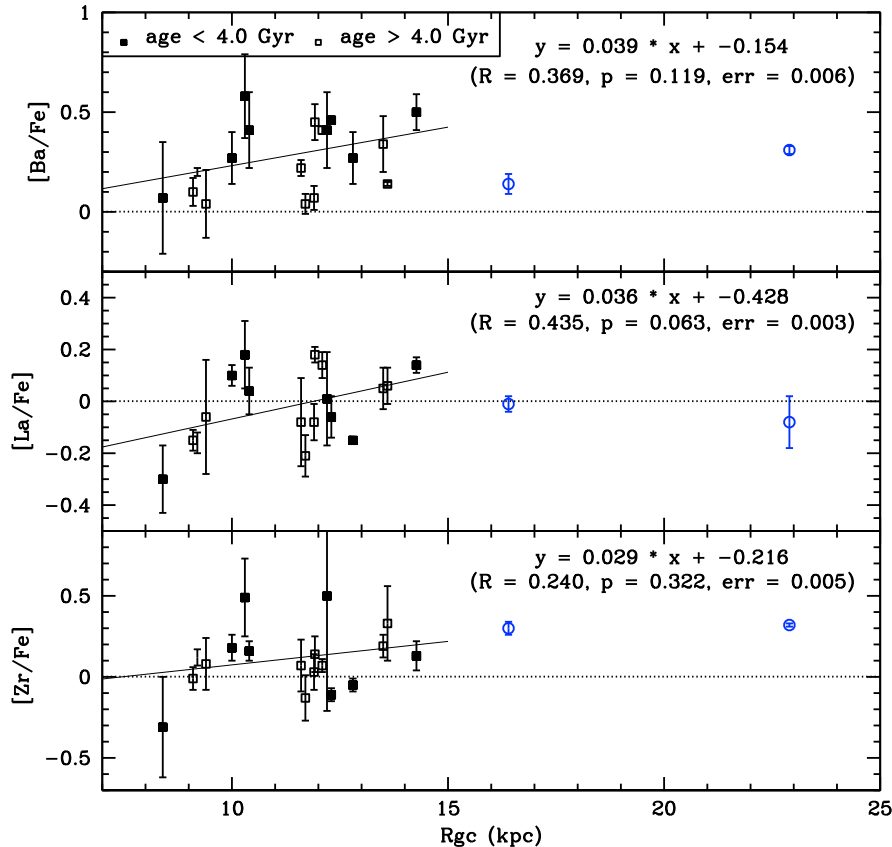


Figure 8. $[\text{s}/\text{Fe}]$ ratios as a function Galactocentric distance. Symbols are the same as in Figure 3. Clusters are distinguished by age: clusters younger than 4 Gyr (filled symbols), clusters 4 Gyr and older (open symbols). In each panel, the line of best fit for *all* clusters within $R_{\text{gc}} < 15$ kpc is indicated, along with its equation, R-value, p-value, and error.

To give an indication of the impact of age uncertainties on the results, we varied the age of the oldest cluster, Be 17, by its uncertainty of 2.77 Gyr as given by the Salaris et al. calibration. This estimate of the uncertainty in age offers an extreme case, both in terms of the Salaris et al. calibration and direct age determinations (e.g., Bragaglia et al. 2006 found an age of 8.5 - 9 Gyr for Be 17 from isochrone fits). Making Be 17's age younger or older both served to slightly decrease the statistical significance of the trends shown in Figure 3, e.g., $p=0.013$ and 0.017 for $[\text{Ba}/\text{Fe}]$. Coupled with the leverage Be 17's large age gives to the fitting of element abundance trends with age, this example provides an indication of the robustness of such trends to age errors. Adopting the more typical 15% age uncertainty of the Salaris et al. calibration would have significantly less impact on any of these correlations.

Lastly, we also performed a regression analysis of our sample's $[\text{X}/\text{Fe}]$ ratios as a function of log age, such as seen in Figure 4, to assess how sensitive the statistical significance of the trends were to how age was represented. We found that, in general, the p-values increased for each element considered here, decreasing the statistical significance of each trend. For example, the p-value of $[\text{Ba}/\text{Fe}]$ versus log age was 0.041, as opposed to 0.010 as seen in Figure 3. However, the opposite is found in an analysis of the D09 sample: the p-value of their clus-

ter $[\text{Ba}/\text{Fe}]$ ratios versus log age was 0.0003, compared to $p = 0.011$ found versus age. This is no doubt due to the much larger age range of the D09 sample relative to ours (the youngest being 35 Myr old, as opposed to our 700 Myr). These changes in p-value do not change the primarily conclusions described above.

4.2. Cluster *n*-capture abundance trends with R_{gc}

The open clusters have often been used as tracers of the elemental abundance distributions in the Milky Way disk. In terms of the traditional characteristics used to categorize disk populations, the properties of the open clusters show overall consistency with those of the thin disk (Friel 1995). Their kinematics, and in particular the systemic rotational properties of the open cluster population, are very similar to those of the thin disk field stars and other disk tracers (Hron 1987; Scott et al. 1995). Cluster ages, spatial distribution, and concentration to the Galactic plane are thin disk-like. As demonstrated by many papers (e.g., Jacobson et al. 2011; Magrini et al. 2009, the elemental abundance ratios of open clusters follow the trends shown by field stars of the thin disk. Although there may be a few open clusters whose individual properties distinguish themselves in interesting ways (e.g. NGC 6791 - Platais et al. 2011; Geisler et al. 2012), the evidence for the open cluster population as a whole is that it provides an important and useful sam-

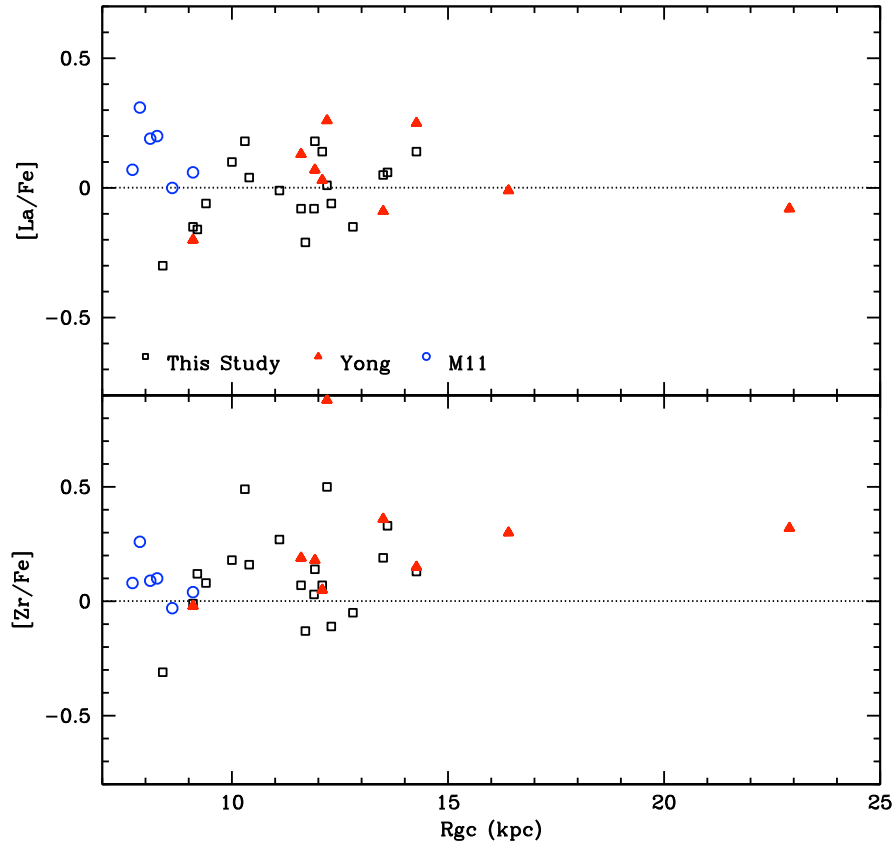


Figure 9. $[s/Fe]$ ratios as a function Galactocentric distance, symbols same as in Figure 5.

ple with which to study the evolution of the thin disk properties.

It is established by now that open clusters (and other disk populations) show that the thin disk’s metallicity gradient, which decreases roughly with a slope of -0.07 dex kpc^{-1} through the solar neighborhood (e.g., Carrera & Pancino 2011), flattens out at $[Fe/H] \sim -0.3$ around $R_{gc} \sim 13$ kpc. Cluster $[X/Fe]$ ratios are essentially flat across the full R_{gc} range spanned by open clusters for the light, α , and Fe-peak elements, indicating that they all follow Fe fairly closely. It is therefore interesting, especially in light of the trends of at least some of them with cluster age, to investigate the trends of n-capture element abundances with R_{gc} . To this end, M11 and Yong et al. (2005, 2012) have all investigated n-capture abundances with R_{gc} . M11 remarked that the s-process elements they studied have distributions similar to the other element groups studied (i.e., α , Fe-peak) – that is, that cluster $[s/Fe]$ is essentially independent of R_{gc} . That said, they note that the trends with R_{gc} for young and old clusters are different, as expected based on the abundance trends with age found in their sample (see, e.g., their Figures 6 and 7 for Ce and Y abundances).

Y12 investigated radial abundance trends in clusters with a focus on distinguishing behavior in the solar neighborhood from that in the outer disk (taken to be $R_{gc} > 13$ kpc). For the neutron-capture elements they find that $[Zr/Fe]$ shows no trend with R_{gc} , but for Ba, La, and Eu, there is a suggestion that the outer disk clusters follow a

different gradient from that of the local sample of clusters. In particular, for La and Eu, the outer disk clusters appear enhanced relative to those inside $\sim 10 - 13$ kpc.

We present $[Ba/Fe]$, $[La/Fe]$ and $[Zr/Fe]$ ratios as a function of cluster R_{gc} for our sample in Figure 8. In each panel, we distinguish older (4 Gyr and greater) and younger (younger than 4 Gyr) clusters by open and filled symbols, respectively, though the details of regression analyses given in each panel is for the entire cluster sample. Given the narrow R_{gc} range of the bulk of our cluster sample ($R_{gc} \sim 8-14$ kpc), we do not draw conclusions about general abundance distributions in the disk as a whole. Rather, we present a linear regression analysis of our original cluster sample alone (with $R_{gc} < 14$ kpc) and include the results in each panel for comparison to the gradients presented by Y12 for what they term the “inner disk” ($R_{gc} < 13$ kpc; their Figure 24). Generally, the gradients we find for $[La/Fe]$ and $[Zr/Fe]$ are larger than those found by Y12, while our slope for $[Ba/Fe]$ is shallower than theirs. None of these slopes are statistically significant. Figure 9 shows $[La/Fe]$ and $[Zr/Fe]$ for our sample along with that of Y12 and M11 as a function of R_{gc} . Again, the distributions of all three samples are consistent with one another.

Figure 10 shows $[Eu/Fe]$ versus R_{gc} , again with the clusters divided into younger (filled symbols) and older (open symbols) age bins. Y12 reported a possible trend of enhanced $[Eu/Fe]$ in the outer disk. However, with their $[Eu/Fe]$ ratios adjusted to our abundance scale, the

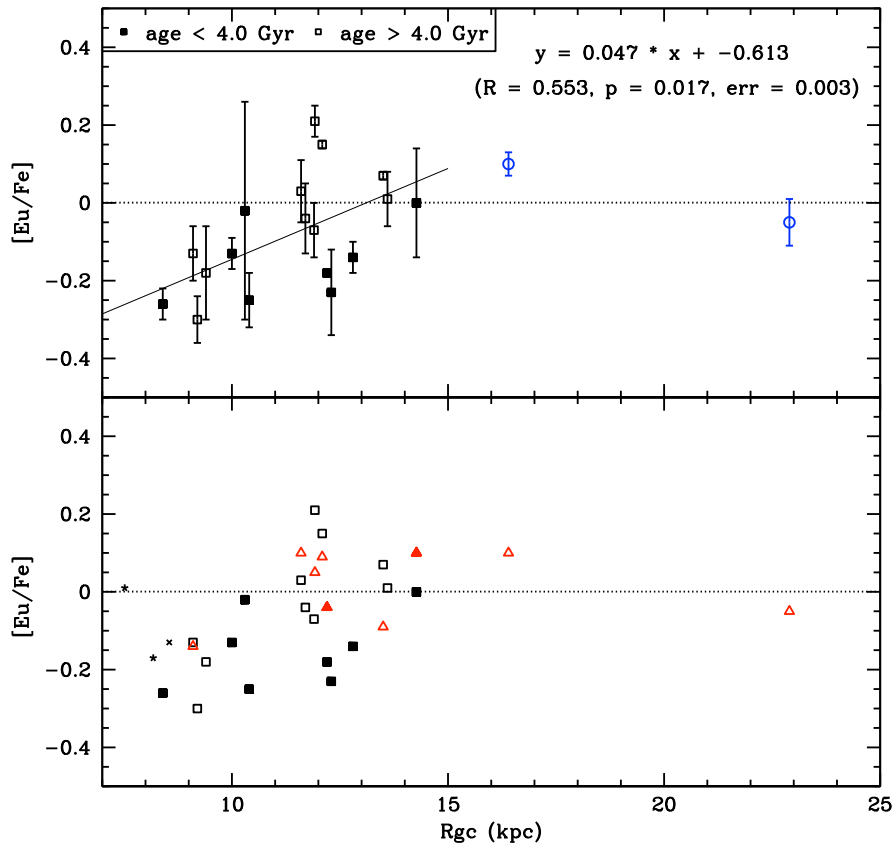


Figure 10. Top panel: $[\text{Eu}/\text{Fe}]$ ratios as a function Galactocentric distance. Symbols same as in Figure 8. Bottom panel: $[\text{Eu}/\text{Fe}]$ ratios versus R_{gc} for our sample (squares), those of Yong et al. (2005, 2012; triangles) shifted to our abundance scale. As in Figure 8, open symbols represent clusters 4 Gyr and older and filled symbols represent clusters younger than 4 Gyr. Smaller points represent clusters from the literature (crosses: age < 4 Gyr; asterisks: age \geq 4 Gyr).

four clusters beyond $R_{\text{gc}} \sim 13$ kpc in their sample have abundance ratios consistent with the inner disk clusters (bottom panel of Figure 10). Therefore, in comparison to the conclusions from Y12, we note that the systematic differences between our abundance scales for $[\text{La}/\text{Fe}]$ (-0.29 dex) and $[\text{Eu}/\text{Fe}]$ (-0.16 dex), when taken into account, would serve largely to remove the differences they see between the inner and the outer disk abundances, yielding trends consistent with those seen in Figures 8 and 10.

That said, the younger and older populations of clusters appear distinct in $[\text{Eu}/\text{Fe}]$ versus R_{gc} (Figure 10). The younger clusters (filled symbols) do not exhibit statistically significant trend with R_{gc} , but the trend with R_{gc} for the older clusters (open symbols) is marginally significant ($p=0.017$). We found, however, that these trends are largely driven by the radial variation of cluster $[\text{Fe}/\text{H}]$ rather than of $[\text{Eu}/\text{H}]$, indicative of a possible flattening of the thin disk abundance gradient over time. It would be interesting to explore possible variations in the radial distributions of younger and older clusters in larger, homogeneous cluster samples that better probe the full R_{gc} and age range of the Galactic disk.

4.3. Other abundance ratio trends

As discussed in earlier sections, barium and lanthanum are both heavy s-process elements, so it seems reasonable

to expect their abundances to scale together. Figure 11 shows $[\text{Ba}/\text{Fe}]$ versus $[\text{La}/\text{Fe}]$ (top panels) for our cluster sample. Here again, we distinguish younger clusters (<4 Gyr) from older clusters (>4 Gyr) with filled and open symbols, respectively. It can be seen from the top left panel that $[\text{Ba}/\text{Fe}]$ and $[\text{La}/\text{Fe}]$ do appear to scale together, though with a constant offset from a 1-to-1 correlation. $[\text{Zr}/\text{Fe}]$ also seems to be well correlated with $[\text{La}/\text{Fe}]$ for most clusters in our sample as well (top right panel). Also, younger clusters in our sample are slightly shifted to higher $[\text{Ba}/\text{Fe}]$ ratios from the older clusters as a result of the $[\text{Ba}/\text{Fe}]$ correlation with age we have already discussed, but with much overlap (especially when errorbars are taken into account).

As Zr is a light s-process element, the ratios of $[\text{Ba}/\text{Zr}]$ and $[\text{La}/\text{Zr}]$ provide information about the efficiency of s-process element production in the AGB stars that enriched the gas from which clusters in the disk formed¹⁴. The bottom panels of Figure 11 shows the ratios of Ba and La to Zr as a function of cluster $[\text{Fe}/\text{H}]$ for our sample with the clusters distinguished by age. Neither age

¹⁴ As mentioned previously, as a light s-process element, Zr can also be produced via the weak s-process in massive stars (e.g., Busso & Gallino 1985). However, as mentioned in Maiorca et al. (2012), the estimated weak s-process contribution to the solar system light element abundance distribution is small (Serminato et al. 2009).

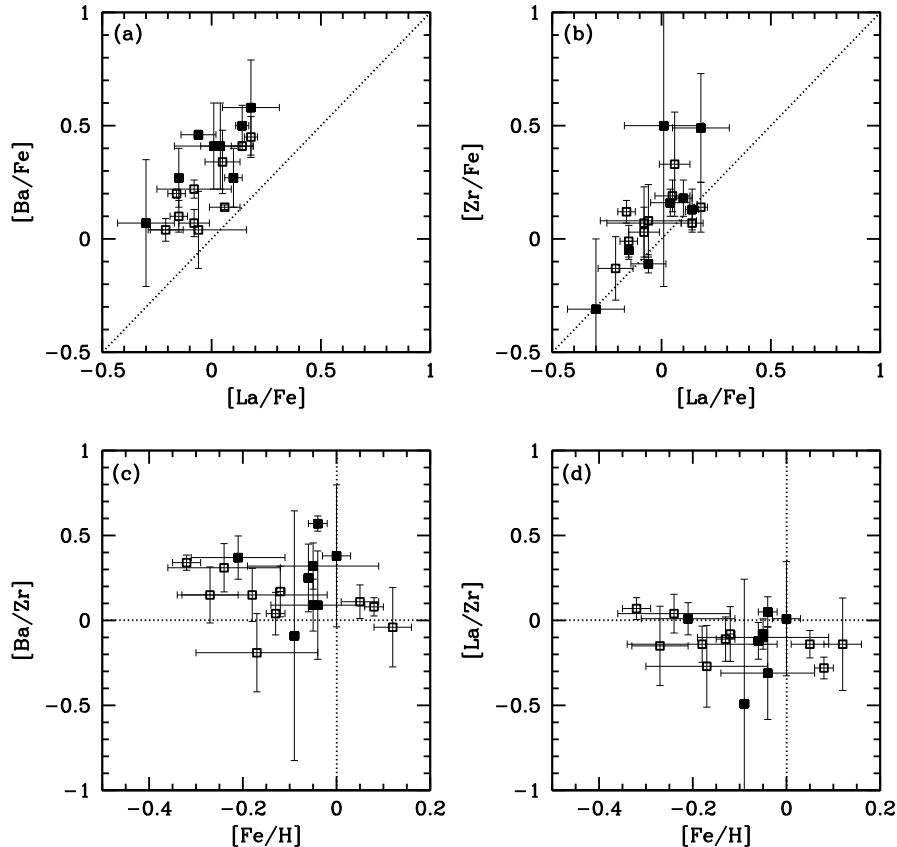


Figure 11. Top panels: $[\text{Ba}/\text{Fe}]$ (a) and $[\text{Zr}/\text{Fe}]$ (b) versus $[\text{La}/\text{Fe}]$ for our sample, with dotted lines indicating the 1-to-1 relation. Bottom panels: $[\text{Ba}/\text{Zr}]$ (c) and $[\text{La}/\text{Zr}]$ (d) versus $[\text{Fe}/\text{H}]$ for our sample. Symbols same as in Figure 8.

group shows a statistically significant trend of $[\text{X}/\text{Zr}]$ with $[\text{Fe}/\text{H}]$. Indeed, for the cluster sample as a whole, these $[\text{hs}/\text{ls}]$ versus $[\text{Fe}/\text{H}]$ trends are rather flat, similar to those found for thin disk dwarf stars in Reddy et al. (2003; their Figure 14). We note that plots of $[\text{Ce}/\text{Y}]$ versus $[\text{Fe}/\text{H}]$ for the M11 sample also show a flat distribution with metallicity. Reddy et al. say, “The similarity of the slopes of $[\text{X}/\text{Fe}]$ versus $[\text{Fe}/\text{H}]$ for light (Sr, Y, Zr) and heavy (Ba, Ce) elements may reflect either unchanging relative contributions from AGB stars or a change in these contributions that is offset by a change in the weak s-process contributions from the massive stars. On the assumption that the AGB stars are the controlling influence, the unchanging abundance ratio of heavy to light elements indicates that the exposures to neutrons in the s-process site is essentially independent of the metallicity of the contributing AGB stars.” If this interpretation is true, it implies that s-process yields of AGB stars do not change as a function of $[\text{Fe}/\text{H}]$ in the metallicity range spanned by our sample, but may still vary as a function of AGB star age (i.e., mass), as mentioned in da Silva et al. (2012). This interpretation is consistent with the model proposed by Maiorca et al. (2012), but again the situation is confused by the uncertainties in the abundance trends with age seen for the heavy and light s-process elements among the various studies.

Figure 12 plots $[\text{Ba}/\text{Fe}]$, $[\text{La}/\text{Fe}]$ and $[\text{Zr}/\text{Fe}]$ versus $[\text{Eu}/\text{Fe}]$ for clusters in this study. In addition, we also

show $[\text{La}/\text{Fe}]$ versus $[\text{Eu}/\text{Fe}]$ for red horizontal branch stars from the study of Afşar et al. (2012). Plots of s-process elements versus r-process elements reveals the relative contributions of the s- and r-processes to the chemical enrichment of the Milky Way disk. Another presentation of $[\text{s}/\text{r}]$ ratios relative to $[\text{Fe}/\text{H}]$ is given in Figure 13. As can be seen in the bottom panel, the older clusters in our sample (open squares) have scaled solar $[\text{La}/\text{Eu}]$ ratios, except for the two clusters with supersolar metallicity (NGC 7142 and NGC 188). The younger clusters, on the other hand, generally show enhanced $[\text{La}/\text{Eu}]$ ratios. A similar pattern is shown for $[\text{Ba}/\text{Eu}]$, too, shifted relative to that for La (recall the top left panel of Figure 11). The distribution of $[\text{La}/\text{Eu}]$ versus $[\text{Fe}/\text{H}]$ is similar to that shown by the RHB stars of Afşar et al. as well, indicating that metal-rich RHB stars are comparable to clusters as tracers of thin disk characteristics, as Afşar et al. conclude. Taken altogether, these figures as well as Figure 7 show the increasing dominance of the s-process to the chemical evolution of the galactic thin disk.

5. SUMMARY AND CONCLUSIONS

The context of this work has been the recently-discovered trends of open cluster neutron capture element abundances with age and R_{gc} . D09 and M11 have identified increasing $[\text{s}/\text{Fe}]$ with decreasing age for open clusters that affects both heavy and light s-process ele-

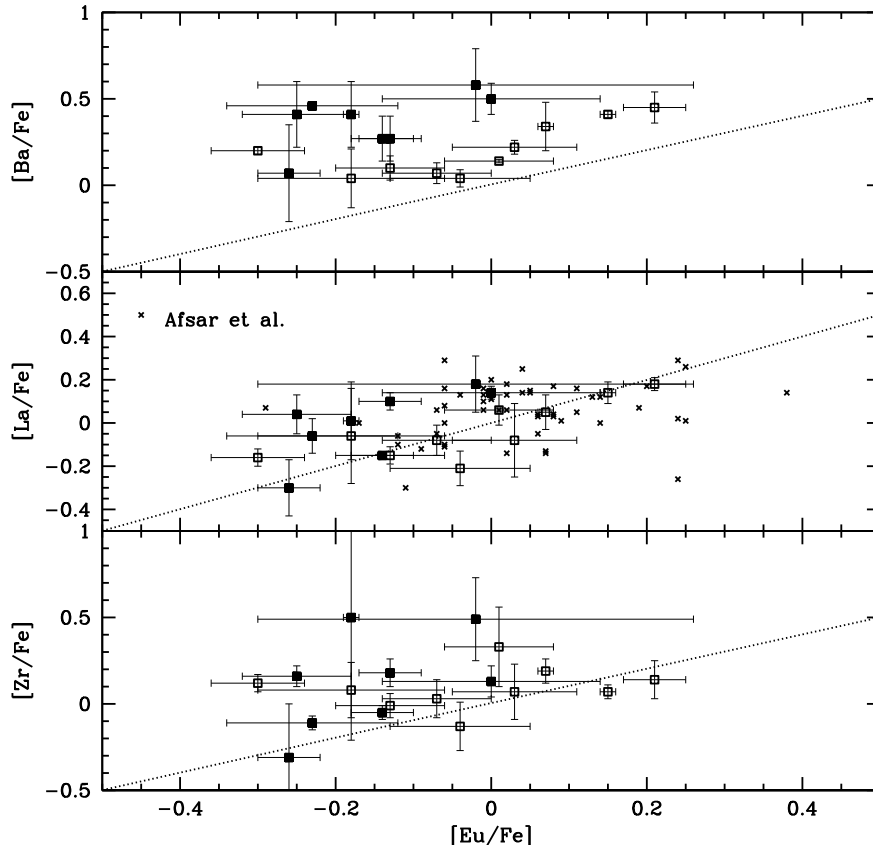


Figure 12. $[X/Fe]$ versus $[Eu/Fe]$ for Ba (top), La (middle) and Zr (bottom). Symbols are the same as in Figure 8, along with field red horizontal branch stars from Afsar et al. (2012) (black crosses) in the middle panels. Dotted lines represent the 1-to-1 relation.

ments; Y12 found such a trend only for Ba. We have also remarked on the analysis of solar neighborhood dwarf stars by da Silva et al. (2012), who also reported trends of increasing $[s/Fe]$ ratios with age, especially for stars younger than 4.5 Gyr, though we noted the contradictory findings of other solar neighborhood field star studies (Reddy et al. 2003; Bensby et al. 2005).

Here, we have presented an analysis of neutron capture element abundances in a sample of 19 open clusters that is completely independent of the open cluster studies described above. In this context, we summarize the results of this work as the following:

- We have found a statistically significant trend of increasing cluster mean $[Ba/Fe]$ with decreasing cluster age, in agreement with D09, Y12 and da Silva et al. (2012).
- In contrast, $[La/Fe]$ and $[Zr/Fe]$ abundances for our sample do not show trends with age. The distribution of $[La/Fe]$ and $[Zr/Fe]$ abundances of the M11 and Y12 samples are not inconsistent with our results.
- We report a marginally significant trend of increasing cluster mean $[Eu/Fe]$ with increasing cluster age for our sample, while trends of $[Ba/Eu]$ and $[La/Eu]$ versus age are statistically significant. This indicates the increase in dominance of

s-process enrichment to the thin disk over time.

- Investigations of $[s/Fe]$ versus R_{gc} for our cluster sample found no statistically significant trends, bearing in mind the limited R_{gc} range of our sample (~ 9 -13 kpc). That said, clusters older than 4 Gyr do show a marginally statistically significant increase in $[Eu/Fe]$ versus R_{gc} that the younger clusters do not. This may be an indication of the flattening of disk abundance gradients with time (Friel et al. 2002; Jacobson et al. 2011).
- The ratio of heavy to light s-process element abundances ($[hs/ls]$) versus $[Fe/H]$ for our cluster sample is flat, consistent with the results of M11 and Reddy et al. (2003) for thin disk dwarfs. One interpretation of this result is that the efficiency of the s-process in AGB stars is independent of their metallicity in this metallicity range, as suggested by Reddy et al. (2003).
- The younger clusters in our sample show enhanced $[s/r]$ ratios compared to the older open clusters, as one might expect based on the trends of individual elements with age discussed above. There is no trend of $[s/r]$ ratio with $[Fe/H]$, again indicating that metallicity does not seem to play a crucial role in evolution of neutron capture elements in open clusters (or more explicitly, in open clusters span-

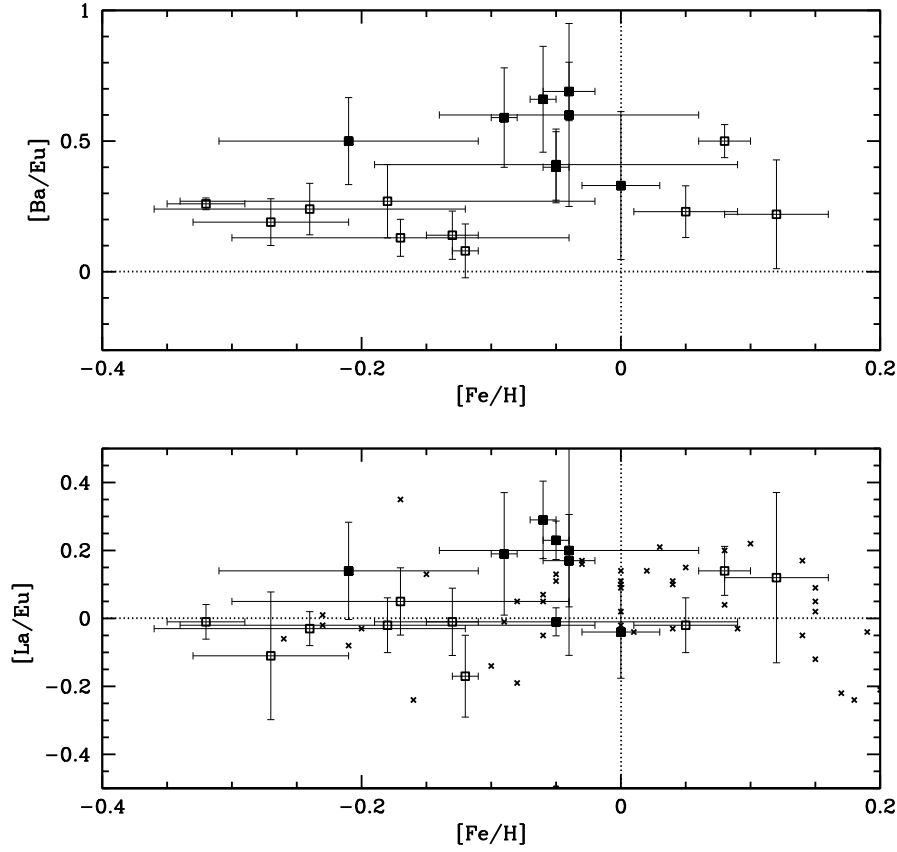


Figure 13. $[\text{Ba}/\text{Eu}]$ (top panels) and $[\text{La}/\text{Eu}]$ (bottom panels) versus $[\text{Fe}/\text{H}]$ for our sample. Symbols are the same as in Figure 8, and again we include the RHB stars from Afşar et al. (2012) as small crosses.

ning the metallicity range of our sample: $[\text{Fe}/\text{H}] \sim -0.30$ to $+0.10$). The clusters' $[\text{s}/\text{r}]$ ratio is also seen to be consistent with other disk populations (RHB stars).

How does one resolve the inconsistencies between the results of this study, D09/M11 and Y12, as well as the inconsistencies in the behaviors of the heavy and light s-process elements? Are these all due to errors or a too-large dispersion in, e.g., our Zr and La abundances that mask trends that are easily seen for Ba? Given the strength of the Ba lines and the sensitivity of the EW measurements to continuum placement and/or blending, as well as their sensitivity to uncertainties in microturbulent velocity, we consider our La measurements to be more reliable. It is possible that the lack of clusters younger than 700 Myr in our sample and in Y12 may limit the detectability of trends with age if only the youngest objects have large enhancements in $[\text{s}/\text{Fe}]$. It is difficult to disentangle the impacts of different age ranges and systematic abundance differences on the conclusions found by different studies. Clearly, it imperative to expand the analysis to include other neutron capture species (both s- and r-process) in not only this sample, but in a larger open cluster sample. We look forward to the Gaia-ESO Survey of stars in many dozens of open clusters that will facilitate the measure of many n-capture species in clusters spanning a wide range in age (Gilmore et al. 2012). We hope that the existence and

strength of any abundance trends with age so far seen (or not) can be verified in a larger, homogeneous study of open cluster chemical abundances.

We gratefully acknowledge the referee for a thoughtful report that improved the presentation of this work. We thank David Yong for sharing reduced spectra of many stars used in this analysis. HRJ thanks Christian Johnson for sharing line lists and for many helpful discussions regarding spectrum synthesis with MOOG, as well as Nick Sterling for many conversations about the s-process. This research has made use of NASA's Astrophysics Data System Bibliographic Services and the Vienna Atomic Line Database. This work has been carried out with support from the National Science Foundation through the NSF Astronomy and Astrophysics Postdoctoral Fellowship under award AST-0901919.

REFERENCES

- Afşar, M., Sneden, C., & For, B.-Q. 2012, *AJ*, 144, 20
 Anders, E., & Grevesse, N. 1989, *Geochim. Cosmochim. Acta*, 53, 197
 Andreuzzi, G., Bragaglia, A., Tosi, M., & Marconi, G. 2004, *MNRAS*, 348, 297
 Asplund, M., Grevesse, N., Sauval, A. J., & Scott, P. 2009, *ARA&A*, 47, 481
 Bell, R. A., Eriksson, K., Gustafsson, B., & Nordlund, A. 1976, *A&AS*, 23, 37

- Bensby, T., Feltzing, S., Lundström, I., & Ilyin, I. 2005, *A&A*, 433, 185
- Bragaglia, A., Tosi, M., Andreuzzi, G., & Marconi, G. 2006, *MNRAS*, 368, 1971
- Burris, D. L., Pilachowski, C. A., Armandroff, T. E., et al. 2000, *ApJ*, 544, 302
- Busso, M., & Gallino, R. 1985, *A&A*, 151, 205
- Busso, M., Gallino, R., Lambert, D. L., Travaglio, C., & Smith, V. V. 2001, *ApJ*, 557, 802
- Busso, M., Gallino, R., & Wasserburg, G. J. 1999, *ARA&A*, 37, 239
- Carrera, R., & Pancino, E. 2011, *A&A*, 535, A30
- da Silva, R., Porto de Mello, G. F., Milone, A. C., et al. 2012, *A&A*, 542, A84
- D’Orazi, V., Magrini, L., Randich, S., et al. 2009, *ApJ*, 693, L31
- Friel, E. D. 1995, *ARA&A*, 33, 381
- Friel, E. D., Jacobson, H. R., & Pilachowski, C. A. 2005, *AJ*, 129, 2725
- . 2010, *AJ*, 139, 1942
- Friel, E. D., Janes, K. A., Tavarez, M., et al. 2002, *AJ*, 124, 2693
- Geisler, D., Villanova, S., Carraro, G., et al. 2012, *ApJ*, 756, L40
- Gilmore, G., Randich, S., Asplund, M., et al. 2012, *The Messenger*, 147, 25
- Grevesse, N., Noels, A., & Sauval, A. J. 1996, in *Astronomical Society of the Pacific Conference Series*, Vol. 99, *Cosmic Abundances*, ed. S. S. Holt & G. Sonneborn, 117
- Gustafsson, B., Edvardsson, B., Eriksson, K., et al. 2008, *A&A*, 486, 951
- Hinkle, K., Wallace, L., Valenti, J., & Harmer, D. 2000, *Visible and Near Infrared Atlas of the Arcturus Spectrum 3727-9300 Å* (San Francisco: ASP)
- Holweger, H., & Mueller, E. A. 1974, *Sol. Phys.*, 39, 19
- Hron, J. 1987, *A&A*, 176, 34
- Jacobson, H. R., Friel, E. D., & Pilachowski, C. A. 2007, *AJ*, 134, 1216
- . 2008, *AJ*, 135, 2341
- . 2009, *AJ*, 137, 4753
- Jacobson, H. R., Pilachowski, C. A., & Friel, E. D. 2011, *AJ*, 142, 59
- Janes, K. A., & Phelps, R. L. 1994, *AJ*, 108, 1773
- Johnson, C. I., Rich, R. M., Kobayashi, C., & Fulbright, J. P. 2012, *ApJ*, 749, 175
- Kupka, F. G., Ryabchikova, T. A., Piskunov, N. E., Stempels, H. C., & Weiss, W. W. 2000, *Baltic Astronomy*, 9, 590
- Lawler, J. E., Bonvallet, G., & Sneden, C. 2001a, *ApJ*, 556, 452
- Lawler, J. E., Wickliffe, M. E., den Hartog, E. A., & Sneden, C. 2001b, *ApJ*, 563, 1075
- Lodders, K., Palme, H., & Gail, H.-P. 2009, *Landolt Börnstein*, 44
- Loebman, S. R., Roškar, R., Debattista, V. P., et al. 2011, *ApJ*, 737, 8
- Magrini, L., Sestito, P., Randich, S., & Galli, D. 2009, *A&A*, 494, 95
- Maiorca, E., Magrini, L., Busso, M., et al. 2012, *ApJ*, 747, 53
- Maiorca, E., Randich, S., Busso, M., Magrini, L., & Palmerini, S. 2011, *ApJ*, 736, 120
- McWilliam, A. 1998, *AJ*, 115, 1640
- Pancino, E., Carrera, R., Rossetti, E., & Gallart, C. 2010, *A&A*, 511, A56
- Peterson, R. C., Dalle Ore, C. M., & Kurucz, R. L. 1993, *ApJ*, 404, 333
- Pignatari, M., Gallino, R., Heil, M., et al. 2010, *ApJ*, 710, 1557
- Platais, I., Cudworth, K. M., Kozhurina-Platais, V., et al. 2011, *ApJ*, 733, L1
- Prochaska, J. X., Naumov, S. O., Carney, B. W., McWilliam, A., & Wolfe, A. M. 2000, *AJ*, 120, 2513
- Reddy, A. B. S., Giridhar, S., & Lambert, D. L. 2012, *MNRAS*, 419, 1350
- Reddy, B. E., Tomkin, J., Lambert, D. L., & Allende Prieto, C. 2003, *MNRAS*, 340, 304
- Roškar, R., Debattista, V. P., Quinn, T. R., Stinson, G. S., & Wadsley, J. 2008, *ApJ*, 684, L79
- Salaris, M., Weiss, A., & Percival, S. M. 2004, *A&A*, 414, 163
- Scott, J. E., Friel, E. D., & Janes, K. A. 1995, *AJ*, 109, 1706
- Serminato, A., Gallino, R., Travaglio, C., Bisterzo, S., & Straniero, O. 2009, *PASA*, 26, 153
- Smith, V. V., Suntzeff, N. B., Cunha, K., et al. 2000, *AJ*, 119, 1239
- Sneden, C., Cowan, J. J., & Gallino, R. 2008, *ARA&A*, 46, 241
- Sneden, C., Kraft, R. P., Prosser, C. F., & Langer, G. E. 1991, *AJ*, 102, 2001
- Sneden, C. A. 1973, PhD thesis, THE UNIVERSITY OF TEXAS AT AUSTIN.
- Tautvaišienė, G., Edvardsson, B., Tuominen, I., & Ilyin, I. 2000, *A&A*, 360, 499
- van Dokkum, P. G. 2001, *PASP*, 113, 1420
- Villanova, S., Baume, G., & Carraro, G. 2007, *MNRAS*, 379, 1089
- Yong, D., Carney, B. W., & Friel, E. D. 2012, *AJ*, 144, 95
- Yong, D., Carney, B. W., & Teixeira de Almeida, M. L. 2005, *AJ*, 130, 597